NASA
Technical
Paper
2733

July 1987

Mach 6 Experimental and Theoretical Stability and Performance of a Cruciform Missile at Angles of Attack up to 65°

Edward R. Hartman
and Patrick J. Johnston

NASA

NASA Technical Paper 2733

1987

Mach 6 Experimental and Theoretical Stability and Performance of a Cruciform Missile at Angles of Attack up to 65°

Edward R. Hartman
Arnold Engineering Development Center
Arnold Air Force Station, Tennessee

Patrick J. Johnston
Langley Research Center
Hampton, Virginia

National Aeronautics and Space Administration

Scientific and Technical Information Office

Summary

Stability, control, and performance characteristics of an axisymmetric, cruciform finned missile were determined experimentally and theoretically at Mach 6. The all-moveable fins, which were deflected up to 20° for both pitch and roll control, were oriented at fin roll angles of 0° and 45°. The angle-of-attack range extended from 20° to 65° to encompass maximum lift.

Good agreement between experiment and theory was achieved with the fins at a fin roll angle of 0°. A maximum lift coefficient of 5.30 was achieved at an angle of attack of 50°. Theory consistently underpredicted experimental values when the fins were at a fin roll angle of 45°. A predicted maximum lift coefficient of 5.10 was exceeded by approximately ten percent. Fin choking occurred at angles of attack greater than 50°, which caused a dramatic reduction in windward fin effectiveness. Negative deflections alleviated the problem, and positive fin deflections exacerbated the choking phenomenon to the extent that pitch-up occurred at high angles of attack. The maximum trimmed lift coefficient for the configuration with the fins at a fin roll angle of 45° was greater than that for the configuration with the fins at a fin roll angle of 0°. However, because of the directional instability of the configuration with fins at a fin roll angle of 45°, both configurations produced a usable maximum trimmed lift coefficient of approximately 5.20.

Introduction

Compared with its supersonic counterpart, a hypersonic tactical missile has a large turning radius for a given load factor, because turning radius is proportional to the square of velocity. At any speed, the minimum turning radius occurs at maximum lift coefficient. For slender supersonic missiles, the maximum load factor is usually determined by structural considerations. For hypersonic missile concepts, which have lower fineness ratios and therefore greater resistance to bending, the maximum load factor (minimum turning radius) is determined by aerodynamic factors such as maximum lift coefficient or the ability to trim at high lift coefficients.

Experimental hypersonic data on missile-like bodies at very high angle of attack—that is, beyond that required for maximum lift—are limited. Reference 1 contains force data at Mach 6.83 on a family of cone-cylinder bodies; however, this reference does not contain any moment data. References 2 and 3 contain data for force, moment, and pressure distribution on axisymmetric bodies at angles of attack up to 60°, but the Mach number range only extends up to 4.63.

Recently developed Euler codes for calculating the aerodynamic characteristics of missiles (ref. 4) fail when pockets of subsonic flow are encountered. Based on tangent-cone impact-theory concepts, subsonic flow occurs on the stagnation line when the flow deflection angle exceeds 53° at Mach 6. Therefore, even a reasonably slender forebody half angle of 15° would limit the range of applicability of these codes to an angle of attack of less than about 38°, which is far below that required to develop maximum lift. As a result of these mathematical and physical constraints, many aerodynamicists resort to Newtonian hypersonic impact methods to predict vehicle high-angle-of-attack forces and moments. Impact methods, of course, imply isolated panels and components with no mutual interference, whereas the actual flow about a finned missile body at high angles of attack has strong interference effects between the body and fins. Impact theory provides a benchmark comparison by which to judge the effectiveness of future theoretical efforts; this was the primary intent for including it in the present report. Extensive comparisons were made with results obtained from the Hypersonic Arbitrary-Body Aerodynamic Computer Program (ref. 5) to provide some guidance for its use on finned bodies at high angles of attack.

The purpose of the present study was to experimentally determine the high-angle-of-attack hypersonic stability and performance of an axisymmetric body with cruciform fins. The configuration had a simple 12°/6° biconic nose. The all-moveable delta-planform fins were oriented at fin roll angles of 0° and 45° and were deflected to obtain pitch and roll. The test angle-of-attack range extended from 20° to 65° to encompass the angle of attack for maximum lift. The angle of sideslip was varied from 0° to −3° to obtain lateral-directional derivatives. The free-stream Mach number was 5.95 and the length Reynolds number was 2.57×10^6. This Reynolds number corresponds to a 15-ft vehicle at Mach 6 and at an altitude of 127 500 ft.

Symbols

C_A axial-force coefficient, $\frac{\text{Axial force}}{qS}$

$C_{A,b}$ base axial-force coefficient, $-\left(\frac{p_b - p_\infty}{q}\right)$

C_D drag coefficient, $\frac{\text{Drag}}{qS}$

C_L lift coefficient, $\frac{\text{Lift}}{qS}$

C_l rolling-moment coefficient, $\frac{\text{Rolling moment}}{qSd}$

C_{l_β} effective dihedral parameter $\frac{\Delta C_l}{\Delta \beta}$, per deg

C_m pitching-moment coefficient, $\frac{\text{Pitching moment}}{qSd}$

$C_{m_{\delta_p}}$ pitching-moment coefficient as a function of pitch-control deflection

C_N normal-force coefficient, $\frac{\text{Normal force}}{qS}$

C_n yawing-moment coefficient, $\frac{\text{Yawing moment}}{qSd}$

C_{n_β} directional stability parameter $\frac{\Delta C_n}{\Delta \beta}$, per deg

C_p pressure coefficient

C_Y side-force coefficient, $\frac{\text{Side force}}{qS}$

C_{Y_β} side-force parameter $\frac{\Delta C_Y}{\Delta \beta}$, per deg

d reference length (maximum body diameter), 1.300 in.

HABP Hypersonic Arbitrary-Body Aerodynamic Computer Program

L/D lift-drag ratio

ℓ body length, 10.827 in.

M free-stream Mach number

p_b base static pressure, psia

p_∞ free-stream static pressure, psia

q free-stream dynamic pressure, psia

S reference area based on body diameter, 1.327 in^2

x_{cg} center of gravity, moment reference point, inches from nose tip

α angle of attack, deg

β angle of sideslip, deg

δ_p pitch-control deflection of fins (negative with leading edge down), deg

δ_r roll-control deflection of fins (positive to provide positive rolling moment), deg

ϕ fin roll angle, deg

Subscripts:

lam laminar boundary layer

max maximum

trim $C_m = 0$

turb turbulent boundary layer

Model nomenclature:

B body

BT_+ body plus fins in "+" configuration, $\phi = 0°$

$BT_\times$ body plus fins in "×" configuration, $\phi = 45°$

Model, Apparatus, and Tests

A photograph of the model is shown in figure 1 and a sketch is presented in figure 2. The model was constructed of stainless steel and attached to a six-component water-cooled strain-gage balance which was sting supported. Base pressures were measured at four locations (3, 6, 9, and 12 o'clock looking upstream), and the balance axial forces were adjusted to a condition in which free-stream pressure acted over the base. Representative base axial-force coefficients calculated from these pressures are shown in figure 3. Because the base pressure tubes were at a constant location, their relative positions to the "+" and "×" fin configurations were different. This difference may account for the discrepancies observed in base axial-force coefficients at high angles of attack.

The model angle of attack was measured on a calibrated scale outside the tunnel by reflecting a point source of light from a prism embedded in the model surface onto the scale. This method accounted for the deflection of the balance and sting under aerodynamic loads.

The tests were conducted in the Langley 20-Inch Mach 6 Tunnel (ref. 6) at a nominal stagnation pressure and temperature of 150 psia and 860°R, respectively. At these conditions the average free-stream Mach number was 5.95.

The fins were numbered 1, 2, 3, and 4 clockwise from the top fin (+) or top right (×) as viewed looking upstream. (See fig. 2.) Pitch deflections were made by deflecting fins 2 and 4 (+) or all fins (×). Roll deflections were made by deflecting fin 2 (leading edge down) and fin 4 (leading edge up) for the "+" configuration and fins 1 and 2 (leading edge down) and fins 3 and 4 (leading edge up) for the "×" configuration. All deflection angles are defined as the value that each individual fin was deflected.

Fin deflections were set outside the tunnel by using a cathetometer and were checked after every test to insure that the settings did not change as a result of the combination of aerodynamic heating and air loads. The fins were held in place by a simple setscrew friction arrangement.

Corrections and Accuracy

Base pressure was measured and axial forces were corrected to a condition for which free-stream pressure acted on the model base. Aerodynamic heating causes the stainless-steel nozzle blocks in this facility to expand slightly during the course of a test, which increases the expansion ratio and stream Mach number. This effect was accounted for by measuring the stream pitot pressure at the beginning and end of each test to determine Mach number. A linear interpolation with time was then made at each test angle of attack to estimate the correct Mach number.

The accuracies of angle of attack and sideslip are $\pm 0.1°$. Fin deflection angle is accurate to $\pm 0.5°$. Mach number is accurate to approximately ± 0.1. Based on repeatability of data and the Force Data Accuracy Calculations Program (ref. 6), the accuracies of the coefficients in this report are estimated to be:

C_N	± 0.17
C_A	± 0.04
C_m	± 0.13
C_n	± 0.03
C_l	± 0.05
C_Y	± 0.06
C_L	± 0.13
C_D	± 0.12

Theoretical Methods

The static aerodynamic forces and moments on the configuration were calculated by using the Hypersonic Arbitrary-Body Aerodynamic Computer Program (HABP) of reference 5. This computer code has numerous options for predicting either windward or leeward pressures as a function of local panel deflection angle. Because of the large flow deflections involved at high angles of attack, modified Newtonian theory with $C_{p,\max} = 1.82$ was used on the windward surfaces of the body and fins; a Prandtl-Meyer expansion from the free-stream direction was used on all leeward surfaces. The justification for using this combination of theories on the body was based primarily on the results shown in reference 1, where the same theory was used on the windward surfaces but stream pressure ($C_p = 0$) was assumed to occur on leeward surfaces. It was noted that, without exception, lift coefficients in reference 1 were underpredicted, ostensibly because leeside forces were not accounted for.

With respect to the fin forces, the above combination is probably as good as any, because the actual flow is so complex and involves, for example, bow-shock intersections with the fins, local flow and gap effects, fin-shock detachment, and separation.

Skin-friction calculations were made by using the Reference Temperature/Spalding-Chi option in the HABP. Both laminar and turbulent boundary-layer skin-friction predictions were obtained.

Results and Discussion

Component Buildup

The longitudinal forces and moments on the body-fin combinations with the undeflected fins are shown in figure 4. Body-alone results are included for reference.

Considering first the body-alone results, the theory predicted the nonlinear normal force with exceptional accuracy over the entire angle-of-attack range. The theoretical pitching moments, however, were more negative than those measured experimentally. This situation suggests that, although the magnitude of the load on the body was correctly predicted, its distribution over the length of the body was not. In part, the difference may be explained by the fact that impact theory does not account for the actual physics of the local flow. For instance, the theory does not consider the expansion waves emanating from the cone-frustum-cylinder corners, which may intersect the bow wave and reflect back on the body as compression waves. On the windward side, these waves may increase or otherwise alter the loading distribution along the body.

To investigate the moment discrepancies of figure 4 in more detail, the windward and leeward meridian-line pressure distributions on a similarly proportional cone-cylinder body were compared with modified Newtonian/Prandtl-Meyer theories. The tabulated experimental data at Mach 4.63 from reference 3 were used in these comparisons at angles of attack of 20°, 40°, and 60°. With respect to pitching moment, the comparisons were inconclusive. For example, over the entire length of the cylindrical afterbody, the experimental pressures were constant and in excellent agreement with the aforementioned theories. On the 9.46° conical forebody, however, modified Newtonian theory consistently underpredicted the pressures on the windward ray by almost the exact amount that the Prandtl-Meyer expansion theory underpredicted the pressures on the leeward ray; as a result of these compensating effects, good normal-force agreement would be expected. Within the experimental accuracy, the pressures along the top and bottom meridian lines were constant, in accordance with impact-theory concepts. Based on this limited comparison, it must be concluded that the present discrepancy between theoretical and experimental pitching moments is related to the configuration.

The addition of the "+" fins increased the normal force and pitching moments, as expected. However, the theoretical fin increments shown in figure 4(a) must be considered entirely fortuitous, because inviscid impact-theory methods cannot account for bow-shock interference, local q effects, and fuselage boundary-layer cross flows which may separate at the fin root.

Both laminar and turbulent skin-friction estimates were made, and it can be seen by the axial-force comparisons in figure 4(a) that the overall agreement was better using the turbulent theory; hence, it is used in the remaining figures.

Figure 4(b) shows that the addition of the "×" fins increased normal force and pitching moment but, unlike the "+" fins, the increments of these fins were substantially underpredicted by modified Newtonian theory. Above an angle of attack of about 50°, these fins exhibited a distinct pitch-up tendency not predicted theoretically. To examine this tendency further, the incremental forces and moments of both the "+" and "×" fins, along with the theoretical results, are shown in figure 5. The agreement between experiment and theory for the "+" fins was mentioned previously. Of greater concern is the fact that, up to about $\alpha = 50°$, the "×" fins have almost twice the effectiveness that was predicted. This force-and-moment contribution peaks at $\alpha = 60°$ and diminishes thereafter.

The theoretical curves in figure 5(b) show the contributions of the windward and leeward pair of fins as well as the summation of all four fins. Much of the area of the leeside fins is shielded by the body at angles of attack; consequently, their actual effectiveness is substantially less than that shown. A previous study (ref. 7) indicated that the effectiveness of leeside fins could be accurately accounted for by simple geometric shielding in which the isolated panel forces are reduced by the ratio of shielded area to planform area. If the contributions of the leeside fins are entirely discounted, the substantial differences between experiment and theory for the windward fins must be ascribed either to large upwash angles, as the local flow curves outboard around the body, or to local q effects in the body flow field. At Mach 6, for either two-dimensional or conical compressions, local dynamic pressures increase to a maximum of about three times the free-stream values for deflection angles near 25° and subsequently diminish for larger deflection angles. Potentially, the contributions of upwash, local q effects, and carry over of fin loads onto the body might account for the differences between experiment and theory shown in figure 5(b).

Schlieren photographs. To aid in understanding the flow behavior about the configuration, especially with the "×" fins, schlieren photographs were taken at angle-of-attack intervals of 10°. In addition, continuous videotapes of the schlieren images were recorded.

Figure 6(a) shows the flow about the isolated body. The vehicle bow shock lies very close to the body and thus approaches pure Newtonian flow conditions, where the shock is assumed to coincide with the body surface. Therefore, it is not surprising that Newtonian theory was able to accurately predict normal force. Another noticeable feature in figure 6(a) is the rapid curvature of the bow shock when it encounters the expansion fan at the body base.

Figure 6(b) shows the flow about the "+" configuration. The bow shock crosses the lower fin at about the midpoint of the exposed semispan and essentially remains there over the entire angle-of-attack range; thus, part of the ventral fin is exposed to free-stream dynamic pressure, and the remainder experiences a varying local dynamic pressure behind the bow shock. As noted previously, local q ratios at Mach 6 may approach three times the free-stream values; consequently local fin loads may be increased by a corresponding amount. Since the schlieren photographs only show a silhouette of the flow in the meridian plane, it could not be determined whether the bow shock crossed the horizontal fins, which are the primary stabilizing surfaces.

Figure 6(c) shows the schlieren photographs of the flow about the "×" configuration. At $\alpha = 35°$, the bow shock in the vertical plane of symmetry is near the projection of the fin tip-chord plane. Thus, it probably intersected the windward fins since they are rolled out 45° from the meridian plane. It is also evident at this angle of attack that the lower fin leading-edge shock is detached from the leading edge.

As the angle of attack increases to 45°, the detached-fin leading-edge shock appears to intersect the main bow shock in the vicinity of the fin tip chord, and the dark streak downstream of the fin suggests either a strong tip vortex (denoting a large panel loading) or a slip line originating at the intersection of the two shocks.

At an angle of attack of 55° (fig. 6(c)), significant changes in the flow pattern about the windward fins are evident and, as noted previously in figure 5(b), the rate of change in fin contribution to normal force abruptly decreases above $\alpha = 50°$. The schlieren photograph shows a bifurcated shock system ahead of the windward fins with a slip line trailing downstream between the fins. A train of disturbances are also seen reflecting between this slip line and the body surface. Strong disturbances from this shock

intersection cross the body in almost a perpendicular direction.

At $\alpha = 65°$ (fig. 6(c)), the intersection of the bow shock and the highly curved fin shock has moved well forward of the fins and the near-perpendicular disturbances crossing the body are stronger. Though it is very difficult to discern, a slip line originating at the shock intersection appears to impinge on the windward side of the body just downstream of the juncture of the fin leading edge and the body. Given the steep slope of the shock waves (the maximum slope of the fin bow wave at $\alpha = 65°$ was about 78°) and the attendant loss in dynamic pressure behind such a strong shock at Mach 6, it is not surprising that there is a precipitous loss in fin effectiveness as shown in figure 5(b).

The changes in flow patterns discussed previously are associated with local flow choking in the vicinity of the windward pair of fins. The phenomenon was first encountered at supersonic speeds and is described in reference 8. A comparison of fin effective angle of attack at the onset of fin choking and fin effective angle of attack at shock detachment was made in reference 9. It was found that, regardless of fin effective angle of attack, fin choking occurred before shock detachment. In relation to the present study, the "×" configuration has to be at an angle of attack greater than 70° to have the fin effective angle of attack equal to that needed (42°) for shock detachment. Choking occurred at $\alpha \approx 55°$ (fig. 6(c)), which is much less than that needed for shock detachment and follows the trends found in reference 9.

Additional schlieren photographs are shown subsequently that illustrate how fin deflections significantly affect the choking phenomenon.

Longitudinal performance. The lift and drag characteristics of the body and body-fin configurations are shown in figure 7. In figure 7(a), both the magnitude and angles of attack for $C_{L,\max}$ on the isolated body and the body with "+" fins were accurately predicted. This was not the case for the "×" configuration (fig. 7(b)); impact theory consistently underpredicted C_L and C_D. In fact, $C_{L,\max}$ was underpredicted by at least 10 percent.

Longitudinal stability. Figure 8(a) shows the longitudinal stability of the isolated body and the "+" configuration. Because of axial symmetry it is assumed that the data for both configurations would pass through the origin. Experiment and theory show that the longitudinal stability is nonlinear and that the aerodynamic center moves aft as the angle of attack increases.

The stability level of the configuration with the "×" fins (fig. 8(b)) was substantially higher than predicted, and there was a pitch-up tendency at the highest values of C_N, where fin choking was encountered.

Lateral-directional stability. Figure 9 shows the effect of adding the fins on the lateral-directional characteristics. Modified Newtonian theory predicted that the "+" configuration would be directionally unstable up to about $\alpha = 15°$. Also, theory predicted that the "+" fins would have a small, but slightly increasing, effect on C_{n_β} as the angle of attack increased. The experimental fin contribution, however, was several times greater than that predicted theoretically; primarily because of increased q effects in the flow field behind the bow shock on the windward fin. In contrast to the results for the "+" fins, the theory significantly overestimated the directional contribution of the "×" fins (fig. 9(b)). Also, the theory showed a continuous increase in C_{n_β} with angle of attack, but the experimental data increased in magnitude up to $\alpha = 35°$ and then remained essentially constant. The increment in yawing moment due to the "×" fins decreased beyond this angle of attack and was negligibly small at $\alpha = 65°$.

Neither fin arrangement produced significant amounts of rolling moment.

Theory predicted that the "×" fins would produce the larger side-force increment, but experimentally, the "+" fins produced the largest increment in side force.

Longitudinal Trim Characteristics

The effect of control deflection on the longitudinal characteristics of the configuration with the "+" fins is shown in figure 10(a). For a center-of-gravity at 0.52ℓ, the configuration can be trimmed to an angle of attack of approximately 29° with $\delta_p = -20°$. In general, the aerodynamic center moved aft at higher angles of attack and followed the theoretical trends except for $\delta_p = 10°$ above an angle of attack of 50°, where the rate of change in normal force, axial force, and pitch was reduced. The reason for this is not clear, but it may be related to the onset of subsonic flow about the fins and reduced fin lift-curve slope.

Trim characteristics with the "×" fins are shown in figure 10(b). Unlike the more systematic and orderly trends exhibited by the "+" fins, the "×" fins showed considerable discrepancies with theory, especially at $\delta_p = 10°$, where the configuration exhibited severe pitch-up. In addition, large discrepancies occurred between experiment and theory in both normal and axial force.

Schlieren photographs. Figure 11 shows schlieren photographs of the "×" fin arrangement with controls deflected 10° and −20°. As noted, the photographs are for −3° sideslip, because a complete set was not available at $\beta = 0°$. The small angle of sideslip had only a minor effect on the shock configuration.

Comparing the shock system about the windward fins for the two deflection angles, it can be seen that positive deflections caused a strong, highly curved bow shock ahead of the fins. This bow shock resulted in the loss in fin effectiveness at high angles of attack and attendant pitch-up seen in the previous figure. At negative fin deflections, the fin shocks are much weaker, the choked flow between the fins is eliminated, and fin effectiveness is retained up to the highest angle of attack.

Effect of control deflections on performance. Figure 12 shows the variation of lift and drag coefficients with angle of attack for various control deflections. For the "+" fins the magnitudes of C_L and C_D were accurately predicted. A maximum lift coefficient of 5.30 occurred at $\alpha = 50°$ and $\delta_p = 10°$. For the "×" fin configuration, the predicted values of C_L and C_D were low. For the "×" fins, $C_{L,\max} = 5.65$ at $\alpha = 50°$ and $\delta_p = 0°$.

Longitudinal stability. Figure 13 shows the longitudinal stability of the configuration with various pitch-control deflections. Significant discrepancies between experiment and theory are evident, especially for negative deflections with the "+" fins (fig. 13(a)) and with all deflections with the "×" fins (fig. 13(b)). These data, along with the lift results of the previous figure, were used to determine the effect of center of gravity on maximum trimmed lift coefficient. The results are given in figure 14, where it may be noted that for a center of gravity of 0.5157ℓ, the "+" fins produced a trimmed $C_{L,\max}$ of 2.90 and the "×" fins developed a trimmed $C_{L,\max}$ of 3.50.

Although the maximum trimmed C_L for the "×" fins was higher than for the "+" fins, this value could not be achieved, because the configuration became directionally unstable for a center of gravity aft of 0.57ℓ. For the "+" fin orientation, the center of pressure for neutral directional stability was always farther aft than the center of pressure for neutral longitudinal stability. Thus, when trim is considered, there is little difference between the two fin arrangements, either in lift attainable ($C_L = 5.20$) or in center-of-gravity position.

Control authority. Figure 15 compares the control effectiveness of the "+" and "×" fins at three typical angles of attack. It is clear from these data that the "×" fins exhibit essentially twice the control power of the "+" fins up to the angle of attack where fin choking occurs. Beyond that angle of attack, the two fin orientations provide about the same control power, as shown by the results at $\alpha = 60°$.

Pitch-control deflection on sideslip derivatives. Figure 16 shows the effect of pitch control on sideslip derivatives. The isolated-panel concept implicit in Newtonian theory predicted negligibly small effects of control deflection for the "+" fins (fig. 16(a)). The only difference in C_{n_β}, for example, would be due to the increments in axial force between the windward and leeward fins. Experimentally, the yawing-moment derivative for the "+" fins reached a value three times the predicted value at $\alpha = 65°$. This discrepancy was largely the result of interactions of the fin on the body producing yawing moments not accounted for by isolated-panel theory.

Theoretically, negative deflections of the "×" fins produced significant reductions in C_{n_β} because of differences in windward and leeward side-force and axial-force coefficients. The experimental data showed the opposite trend and, in general, failed to follow the theoretical trend as angle of attack increased. The discrepancies in experimental and theoretical C_{n_β} illustrated for the "×" fins in figure 16(b) clearly show the inadequacies of the theory, point out the complex nature of the flow about the "×" fins, and emphasize the need for further investigations of the body-fin interaction problem with the fins at intermediate roll angles ($0° \le \phi \le 45°$).

Differential control deflection. Both fin configurations were tested in pitch with controls deflected differentially to obtain rolling moment. However, as the result of an oversight, only the horizontal fins were deflected for the "+" fin configuration; all four fins were deflected in the "×" configuration. Also, the computer geometry program employed to describe the deflected fin coordinates (GEMPAK, ref. 10) employs a mirror-image concept; that is, only half the vehicle geometry is described. The principal defect with that concept was encountered here with the "×" fins deflected to produce roll. The GEMPAK program cannot account for that situation and, indeed, cannot account for the differential deflections of the horizontal fins in the "+" orientation. In this case, the isolated-fin theoretical data were hand-manipulated to obtain roll, yaw, and side forces.

It can be seen in figure 17(a) that the theory predicted the value of rolling moment with reasonable accuracy. Yawing moments were grossly

underpredicted by factors approaching 4. Similarly, while theory predicted negligible side-force values, significant values of C_Y were measured experimentally. These forces and the resulting yawing moments were clearly caused by side loads induced on the body by the fins and not accounted for theoretically by isolated-panel methods.

As a result of the problems encountered with GEMPAK, no theory results are shown in figure 17(b) for the "×" fin arrangement. Also, because of the oversight mentioned previously, the data for the two fin arrangements are not comparable. The large variations of lateral-directional parameters with angle of attack for the "×" fin orientation (fig. 17(b)) were caused by the cumulative effects of the complex flow phenomena that were alluded to previously, such as shielding, choking, separation, shock impingement, and crossflows. In any event, impact-theory methods would not account for these effects.

Flat-turn radius and load factors. Because the minimum angle of attack for the tests was limited to 20°, neither the trimmed $(L/D)_{max}$ nor the C_L at which it occurred could be determined; nevertheless, extrapolations of the data indicated that this C_L would be about 1.00. From figure 14(a) it can be seen that, for a center of gravity of 0.52ℓ, the maximum trimmed lift coefficient is 2.90. This C_L would allow a Mach 6 turn radius of approximately 68 n.mi. for a 21-in.-diameter missile weighing 1500 lb and flying at the altitude (100 000 ft) for best trimmed L/D. If the center of gravity were moved to 0.60ℓ and the vehicle trimmed at $C_{L,max}$, the turn radius would be reduced by the inverse of the lift-coefficient ratio or to approximately 36 n.mi. Higher air densities at lower altitudes would substantially reduce these values.

Figure 18 shows the precipitous reduction in maximum available load factor with altitude. For certain missions when range is important, a missile may have to fly out at the C_L for $(L/D)_{max}$ (near an altitude of 100 000 ft in this case) then pitch down to altitudes where most aircraft operate (i.e., below about 50 000 ft). Here the vehicle would most likely encounter load factors in excess of 50 g. ($1g = 32.17$ ft/sec^2.)

Conclusions

An experimental and theoretical study was conducted to determine the stability and performance characteristics of cruciform missile configurations at Mach 6. The model had a simple cylindrical fuselage and a 12°/6° biconic nose. Component buildup and control deflection results led to the following conclusions:

1. Longitudinal forces and moments could be accurately predicted on the configuration with the "+" fins using modified Newtonian theory on the windward surfaces of the body and fins and a Prandtl-Meyer expansion from free stream on the leeward surfaces.
2. Serious discrepancies occurred between experiment and theory when the fins were in the "×" orientation where, below $\alpha = 50°$, the theory underpredicted the fin contribution by 50 percent.
3. Above an angle of attack of 50°, the "×" fin contribution to lift and pitching moment diminished precipitously as a result of local flow choking between the body and the windward fins.
4. Fin deflection had a large effect on the occurrence of the choking phenomena; negative deflections tended to alleviate the problem, and positive deflections tended to exacerbate the effects to the extent that pitch-up occurred at high angles of attack.
5. Theory accurately predicted the maximum lift coefficient for the "+" fin arrangement and the angle of attack at which it occurred.
6. Maximum lift coefficient with the "×" fins was underpredicted by at least 10 percent.
7. The "+" configuration exhibited increasingly positive directional stability at angle of attack with values about three times those of the "×" configuration.
8. The "×" fins had about double the control authority in pitch as the "+" fins up to the angle of attack for onset of fin choking.
9. The maximum trimmed lift for the "×" fin arrangement was about 14 percent higher than for the "+" fin arrangement, but this trimmed lift was unusable because the configuration became directionally unstable. Thus, when directional stability was taken into consideration, both fin arrangements produced a maximum trimmed lift coefficient of about 5.20.

NASA Langley Research Center
Hampton, VA 23665-5225
May 19, 1987

References

1. Penland, Jim A.: *Aerodynamic Force Characteristics of a Series of Lifting Cone and Cone-Cylinder Configurations at a Mach Number of 6.83 and Angles of Attack up to 180°*. NASA TN D-840, 1961.
2. Landrum, Emma Jean; and Babb, C. Donald: *Wind-Tunnel Force and Flow-Visualization Data at Mach Numbers From 1.6 to 4.63 for a Series of Bodies of Revolution at Angles of Attack From −4° to 60°*. NASA TM-78813, 1979.

3. Landrum, Emma Jean: *Wind-Tunnel Pressure Data at Mach Numbers From 1.6 to 4.63 for a Series of Bodies of Revolution at Angles of Attack From -4° to 60°*. NASA TM X-3558, 1977.
4. Wardlaw, A. B., Jr.; Baltakis, F. P.; Solomon, J. M.; and Hackerman, L. B.: *An Inviscid Computational Method for Tactical Missile Configurations*. NSWC TR 81-457, U.S. Navy, Dec. 1, 1981.
5. Gentry, Arvel E.; and Symth, Douglas N.: *Hypersonic Arbitrary-Body Aerodynamic Computer Program (Mark III Version)*. Rep. DAC 61552 (Air Force Contract Nos. F33615 67 C 1008 and F33615 67 C 1602) McDonnell Douglas Corp., Apr. 1968. *Volume I—User's Manual.* (Available from DTIC as AD 851 811.) *Volume II—Program Formulation and Listings.* (Available from DTIC as AD 851 812.)
6. Keyes, J. Wayne: *Force Testing Manual for the Langley 20-Inch Mach 6 Tunnel.* NASA TM-74026, 1977.
7. Johnston, Patrick J.; and Hartman, Edward R.: *Experimental and Theoretical Performance and Stability of an Airbreathing Missile Concept at Mach Numbers From 3.5 to 6.0.* NASA TP-2647, 1987.
8. Stallings, Robert L., Jr.; Lamb, Milton; and Watson, Carolyn B.: *Effect of Reynolds Number on Stability Characteristics of a Cruciform Wing-Body at Supersonic Speeds.* NASA TP-1683, 1980.
9. Stallings, R. L., Jr.: Effect of Reynolds Number on the Aerodynamic Characteristics of a Cruciform Wing-Body Configuration. AIAA Paper 79-0301, Jan. 1979.
10. Stack, Sharon H.; Edwards, Clyde L. W.; and Small, William J.: *GEMPAK: An Arbitrary Aircraft Geometry Generator.* NASA TP-1022, 1977.

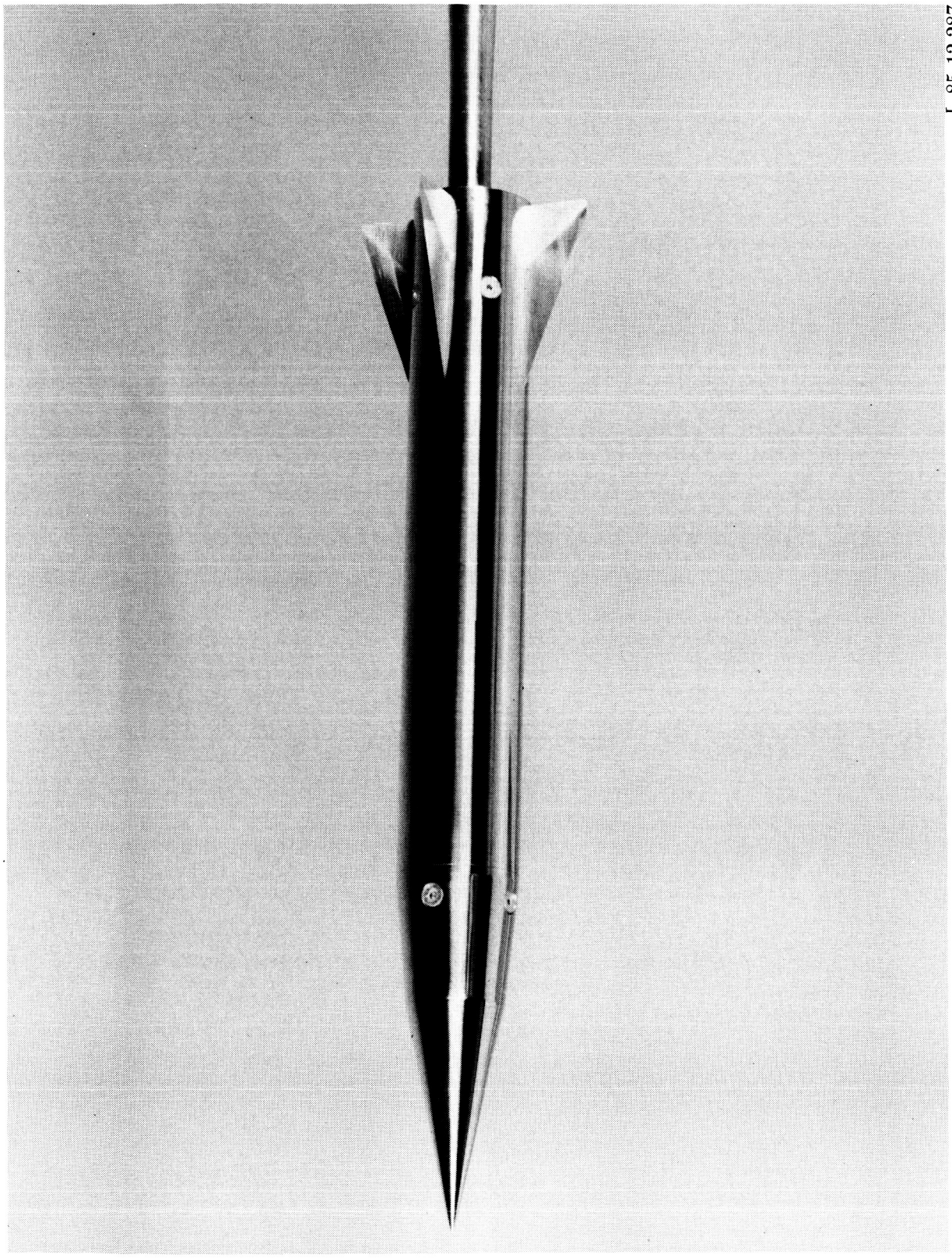

L-85-12,287

Figure 1. Photograph of model.

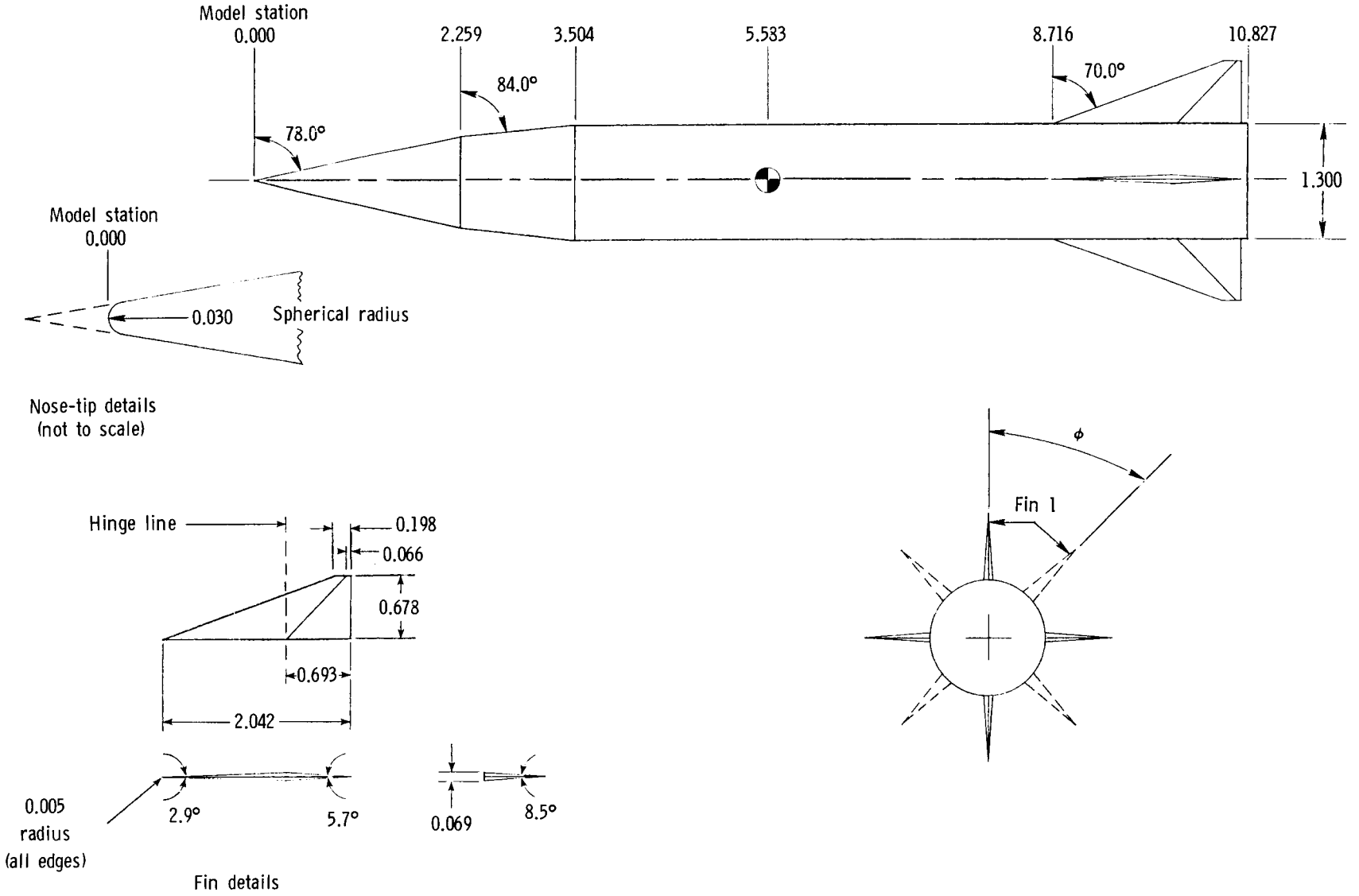

Figure 2. Sketch of model. All linear dimensions in inches.

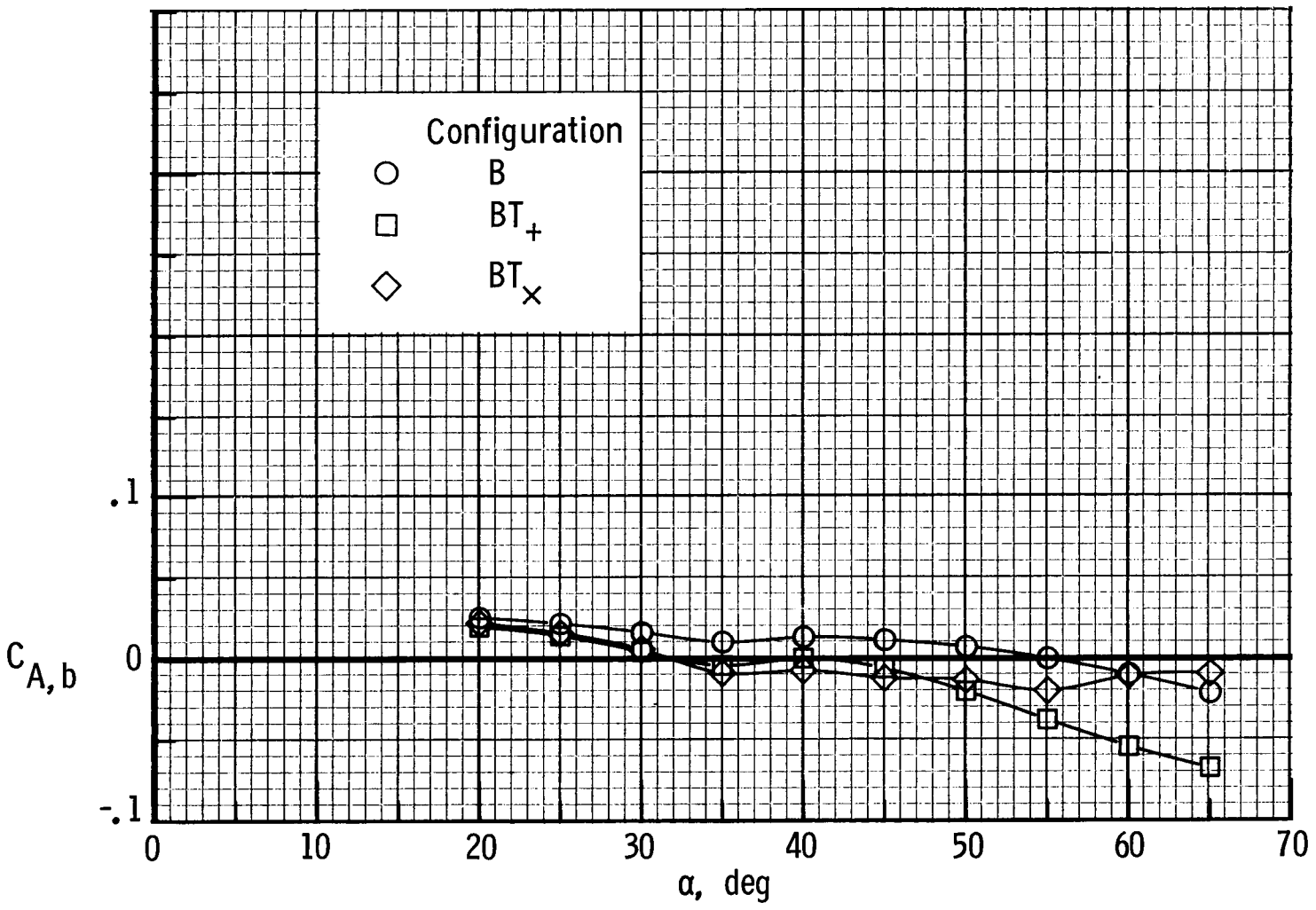

Figure 3. Representative base axial-force coefficients for $\delta_p = 0°$.

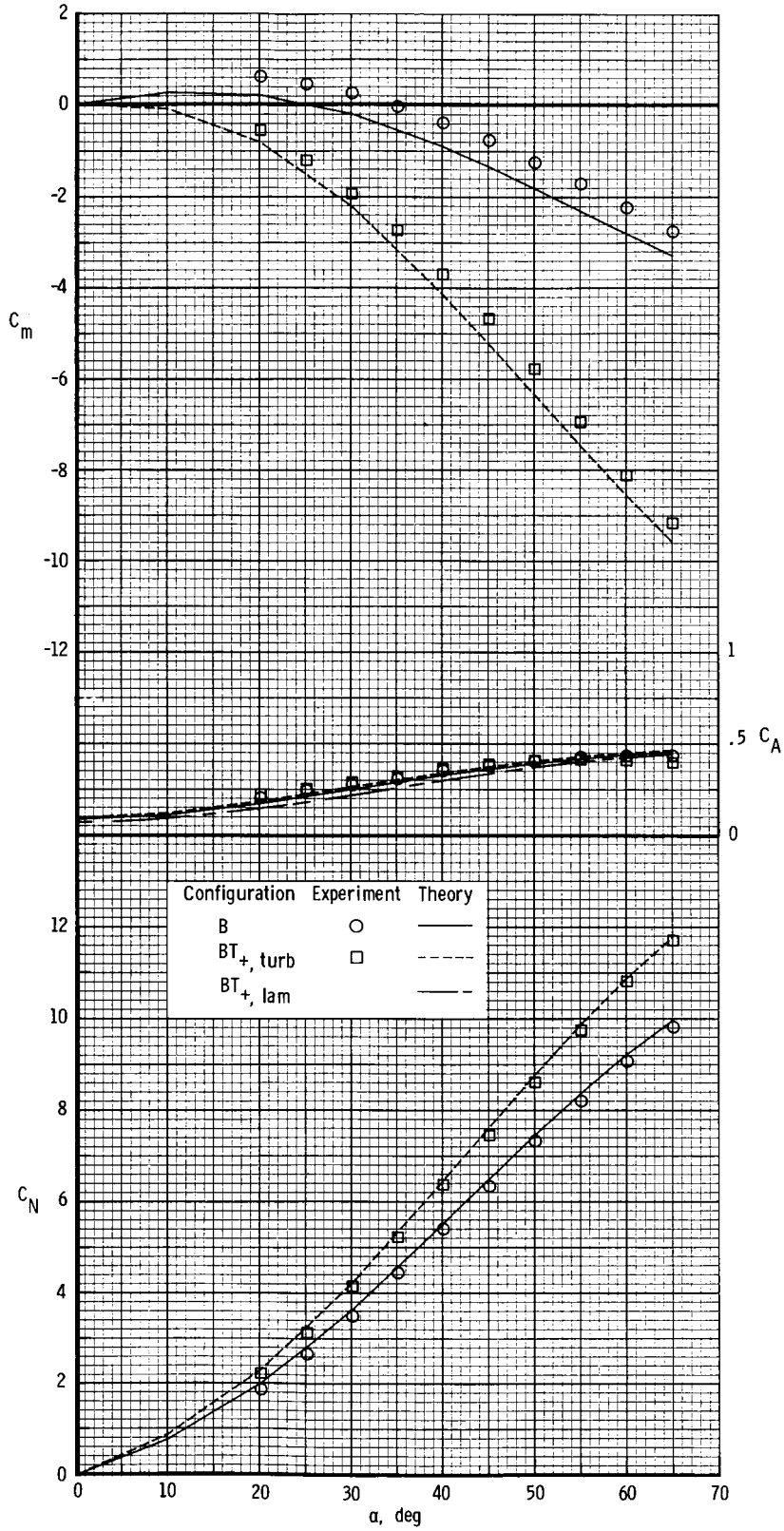

(a) "+" fins.

Figure 4. Effect of component buildup on longitudinal aerodynamic characteristics for $\delta_p = 0°$.

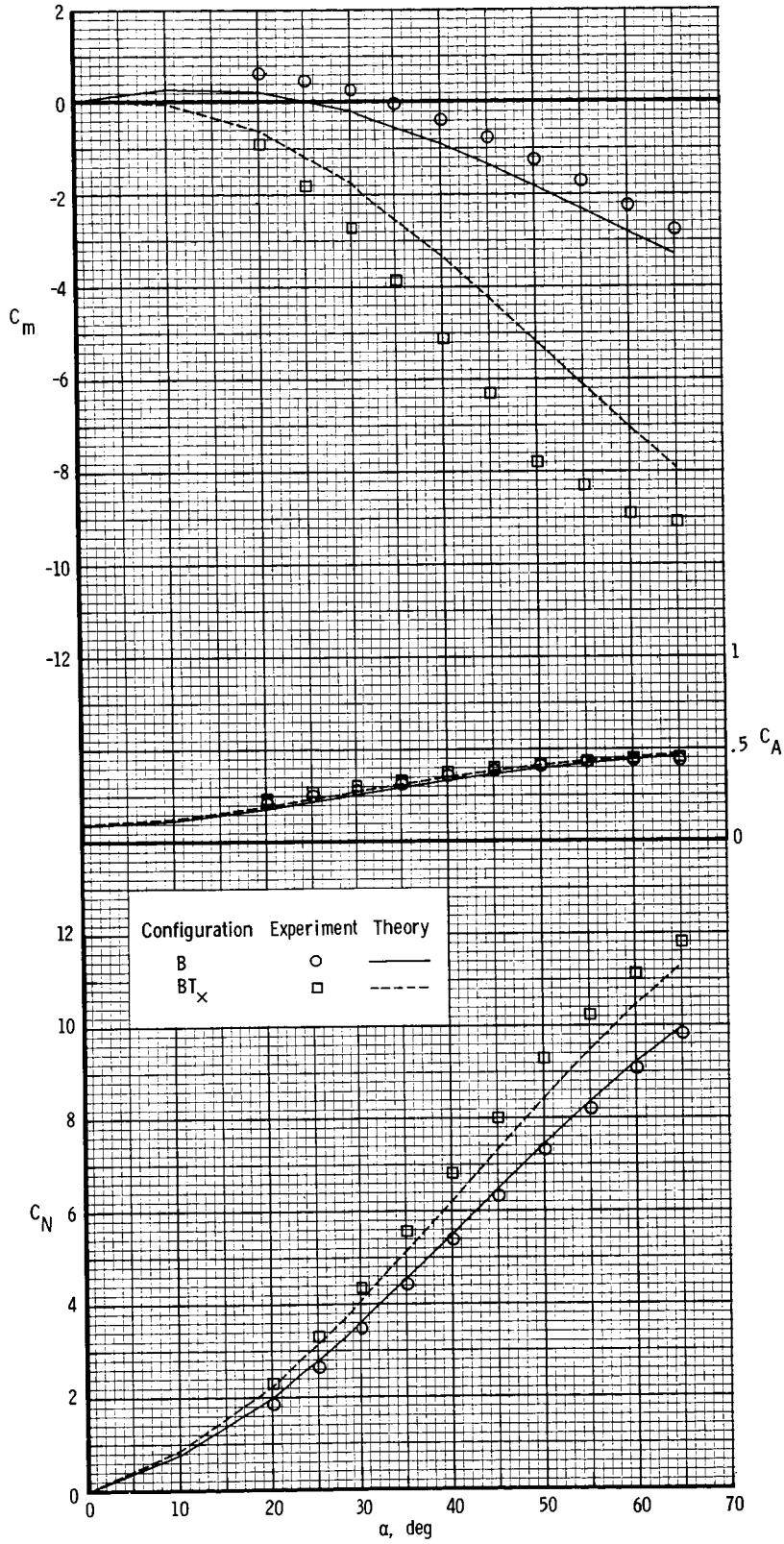

(b) "×" fins.

Figure 4. Concluded.

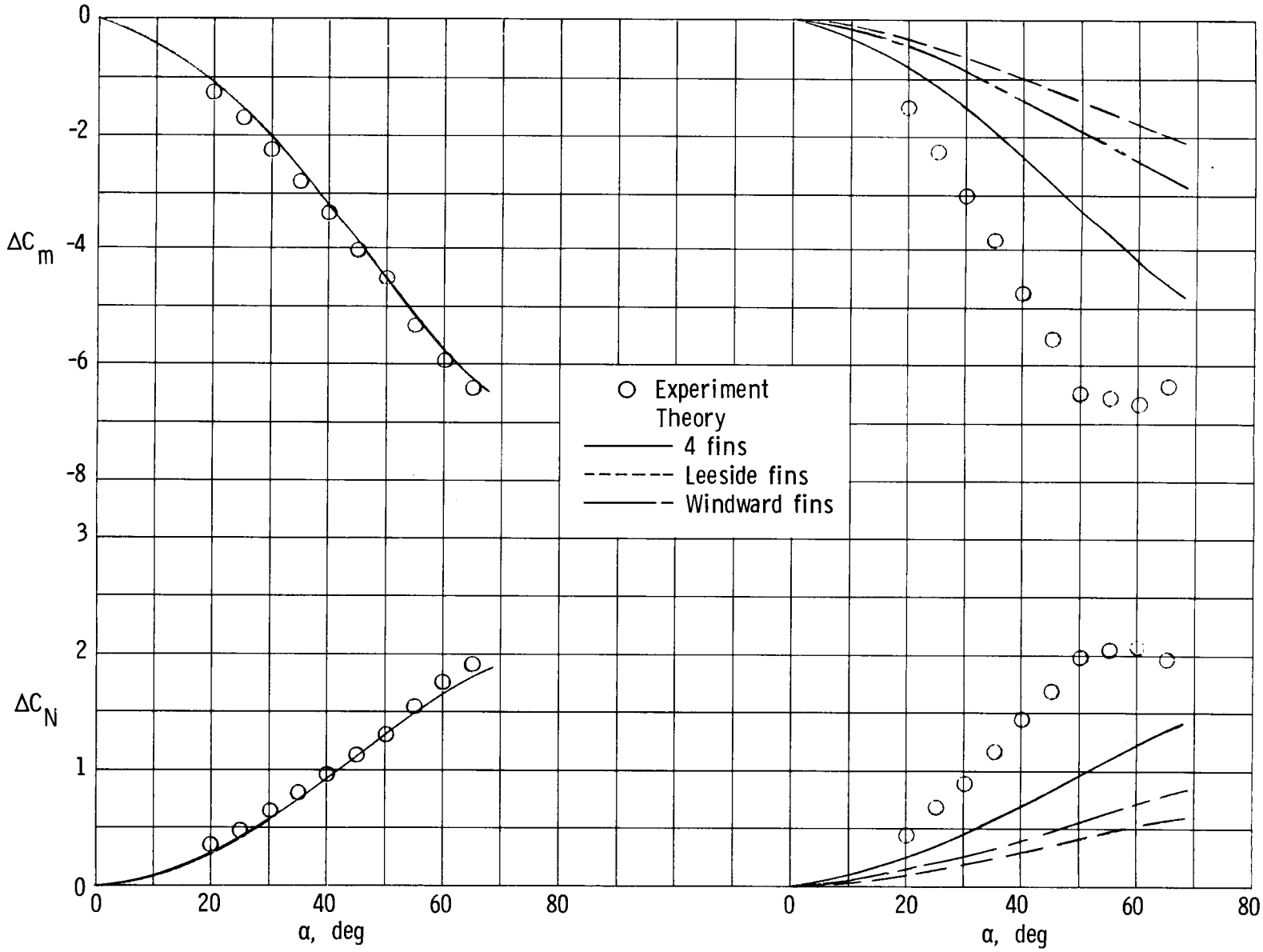

(a) "+" fins.

(b) "×" fins.

Figure 5. Incremental fin contribution on longitudinal aerodynamic characteristics for $\delta_p = 0°$.

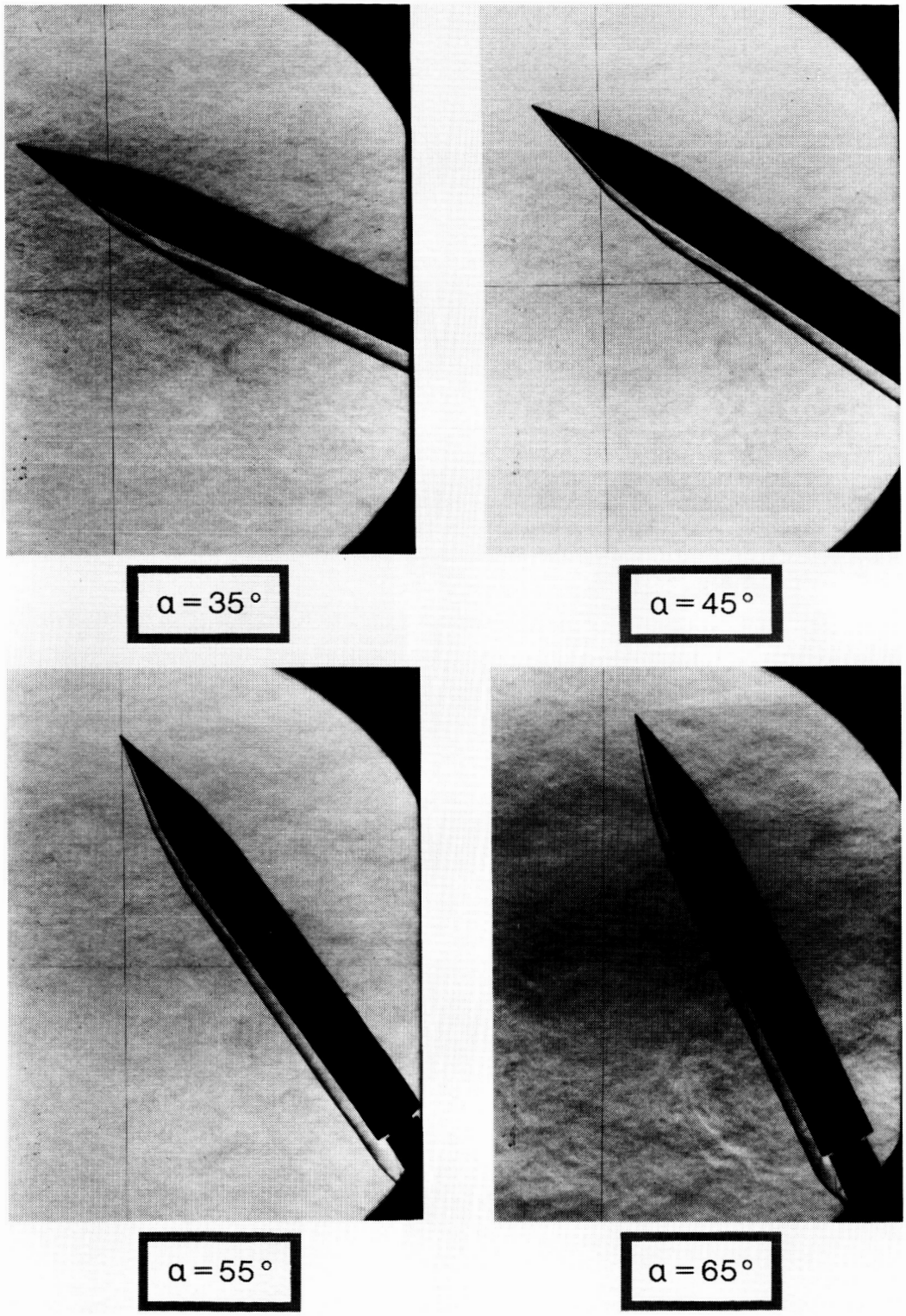

(a) Body alone.

Figure 6. Schlieren photographs of various configurations.

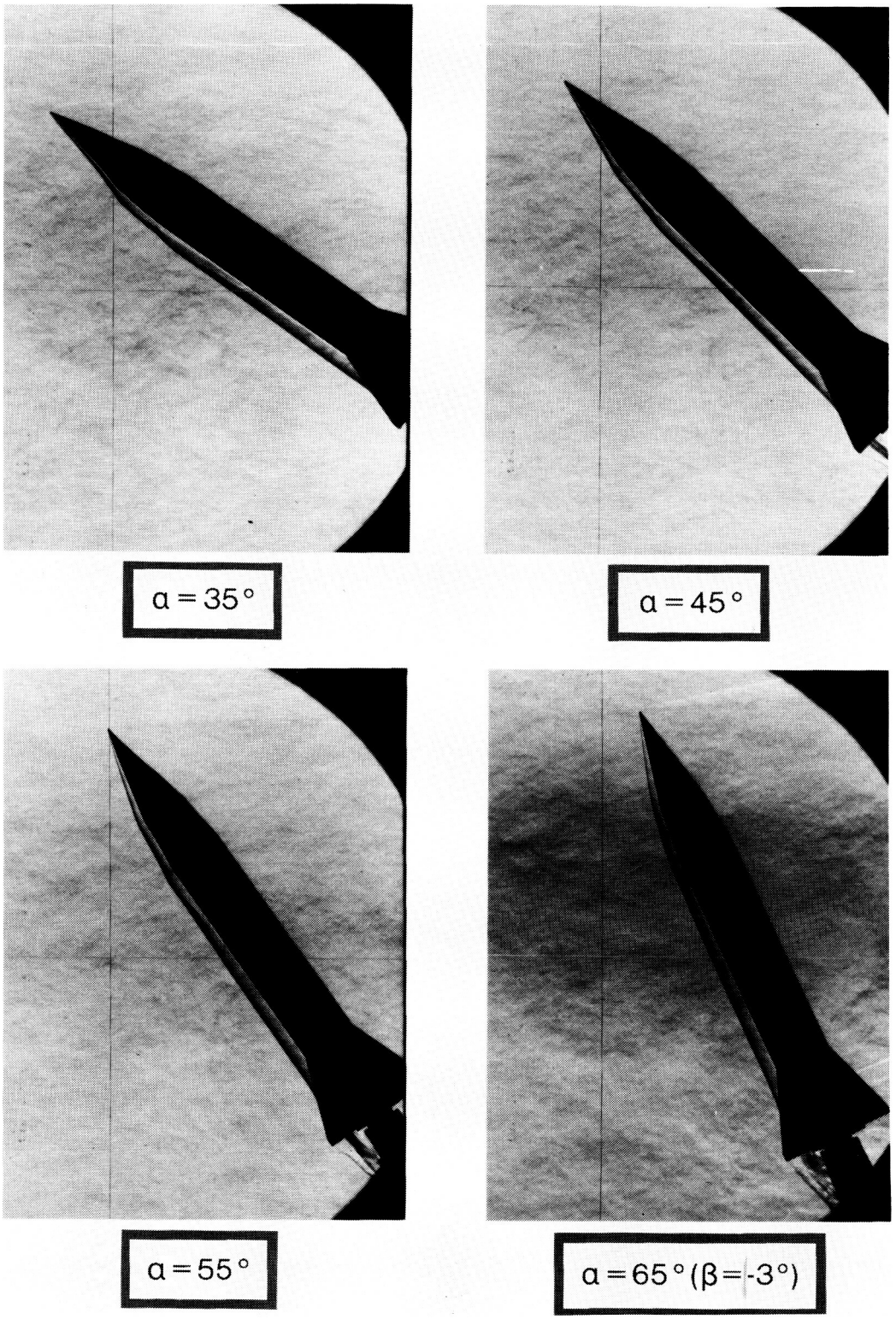

(b) "+" fins, $\delta_p = 0°$.

Figure 6. Continued.

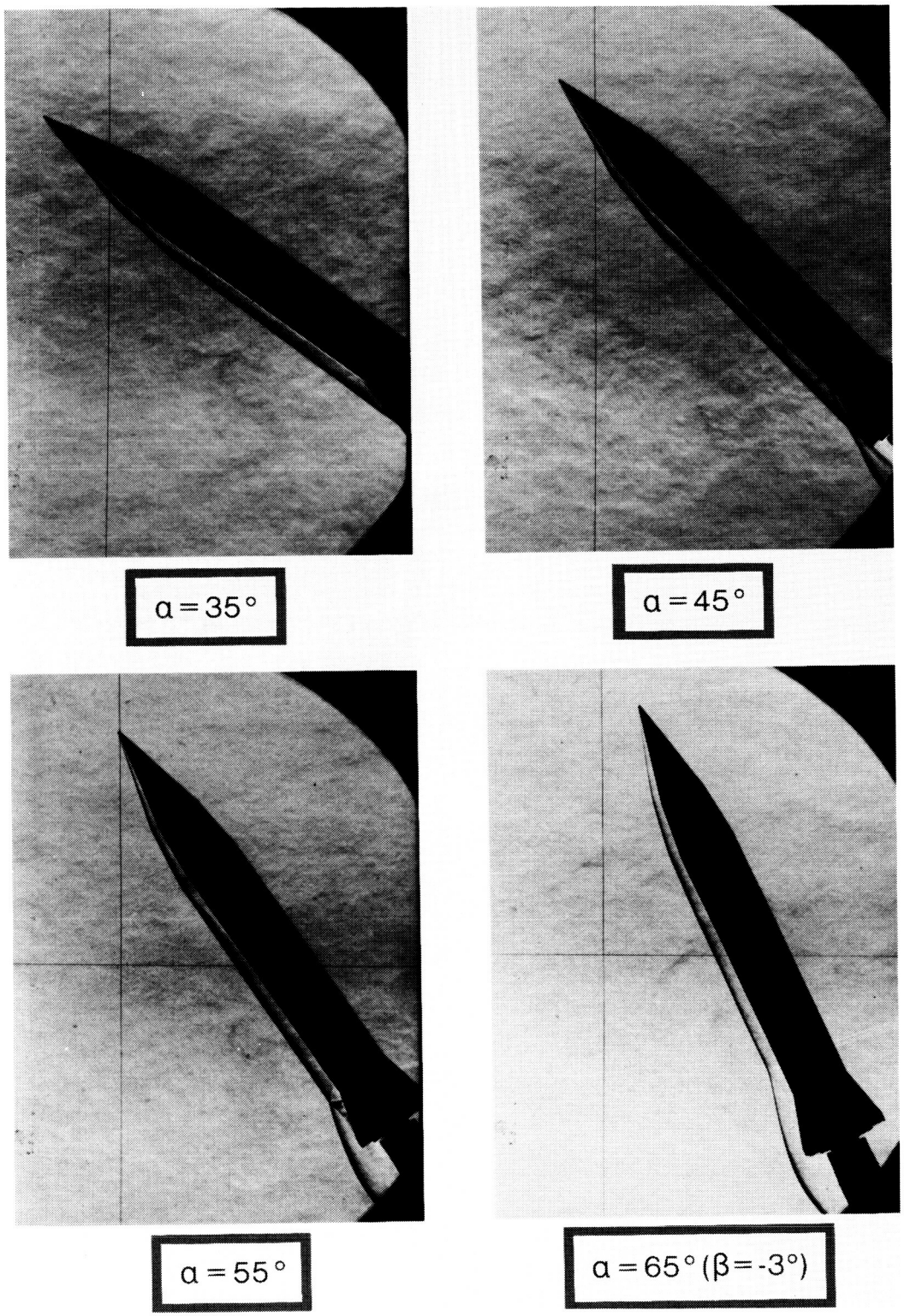

(c) "×" fins, $\delta_p = 0°$.

Figure 6. Concluded.

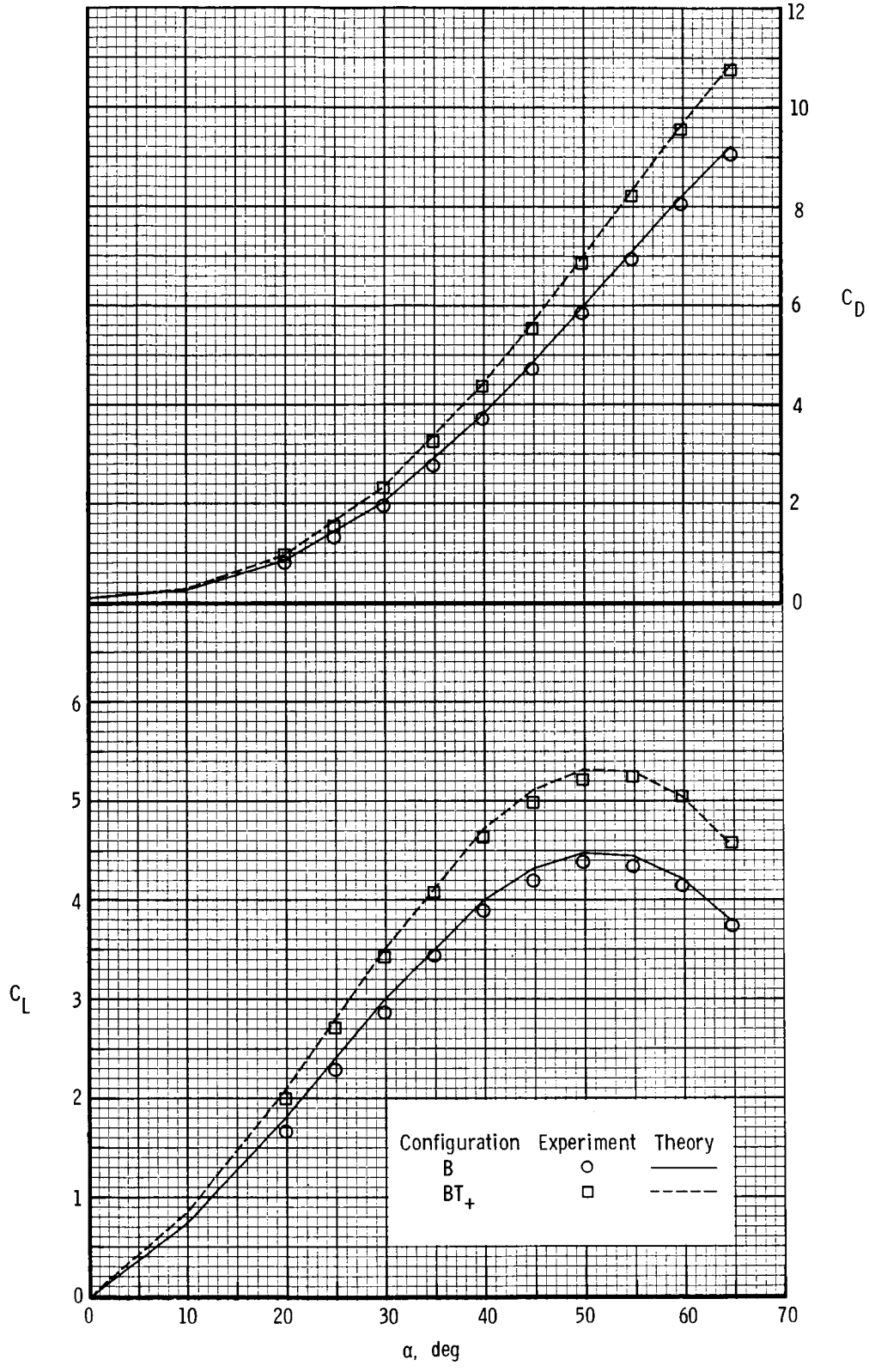

(a) "+" fins.

Figure 7. Effect of component buildup on performance characteristics for $\delta_p = 0°$.

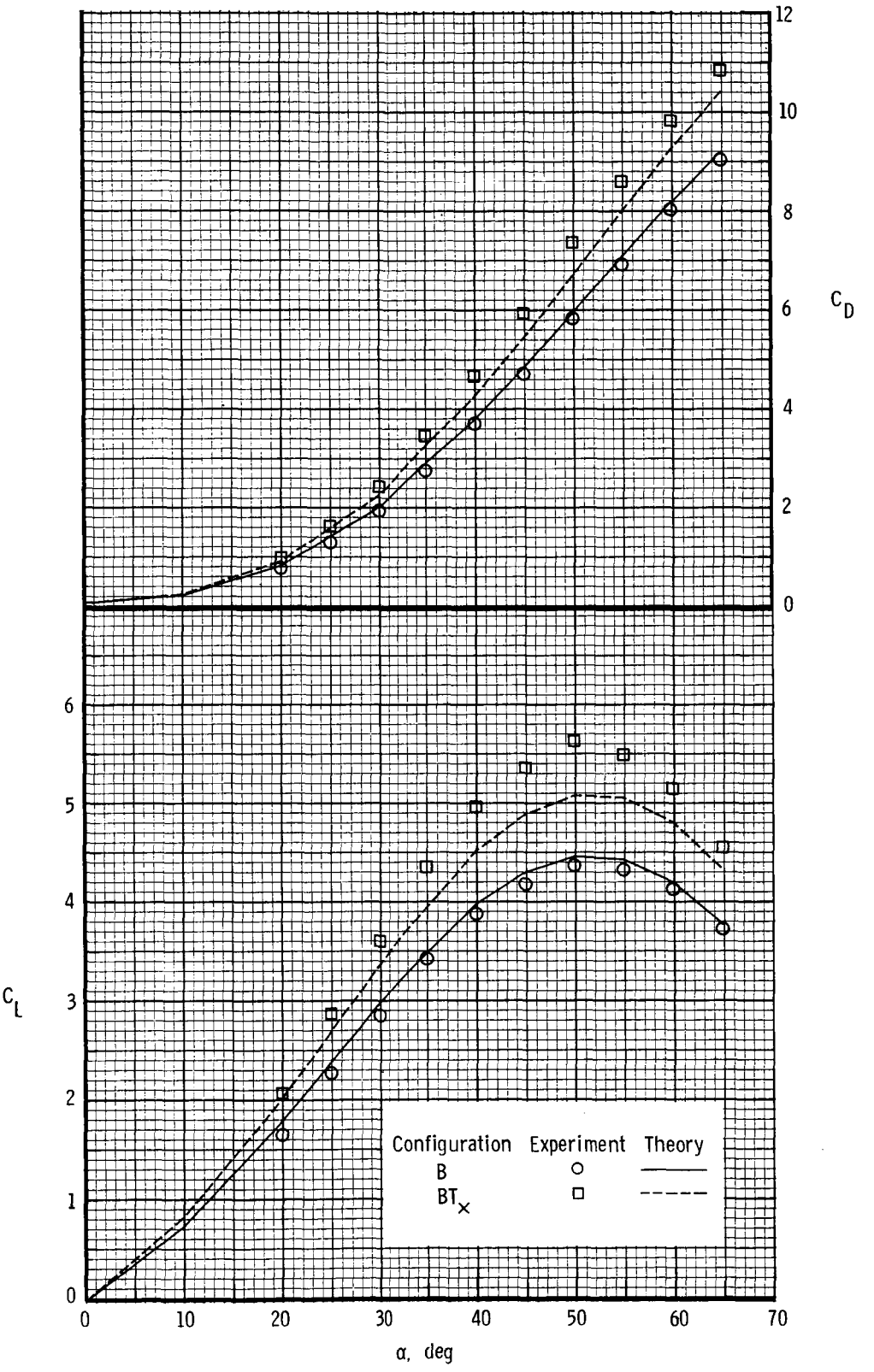

(b) "×" fins.

Figure 7. Concluded.

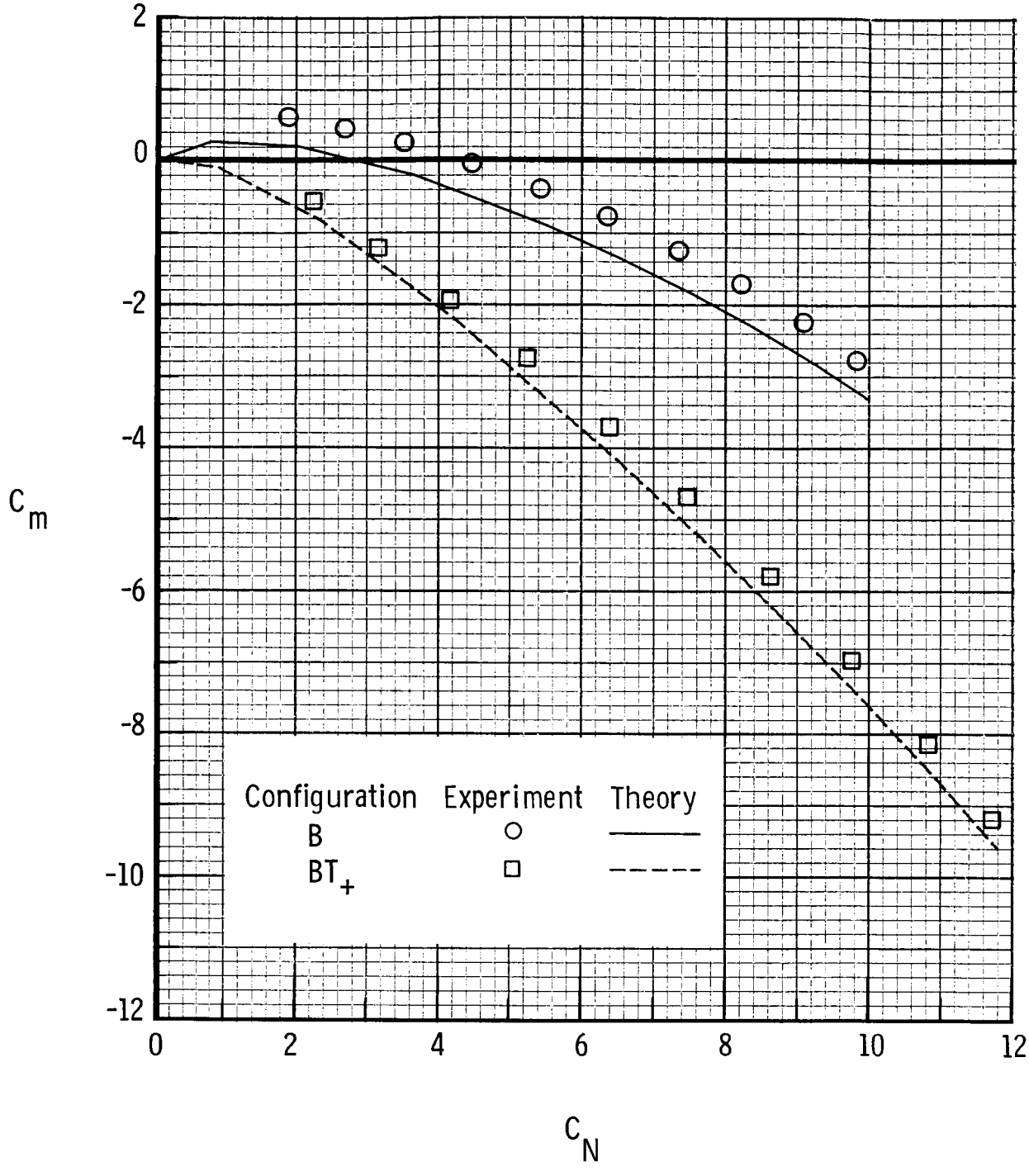

(a) "+" fins.

Figure 8. Effect of component buildup on longitudinal stability for $\delta_p = 0°$.

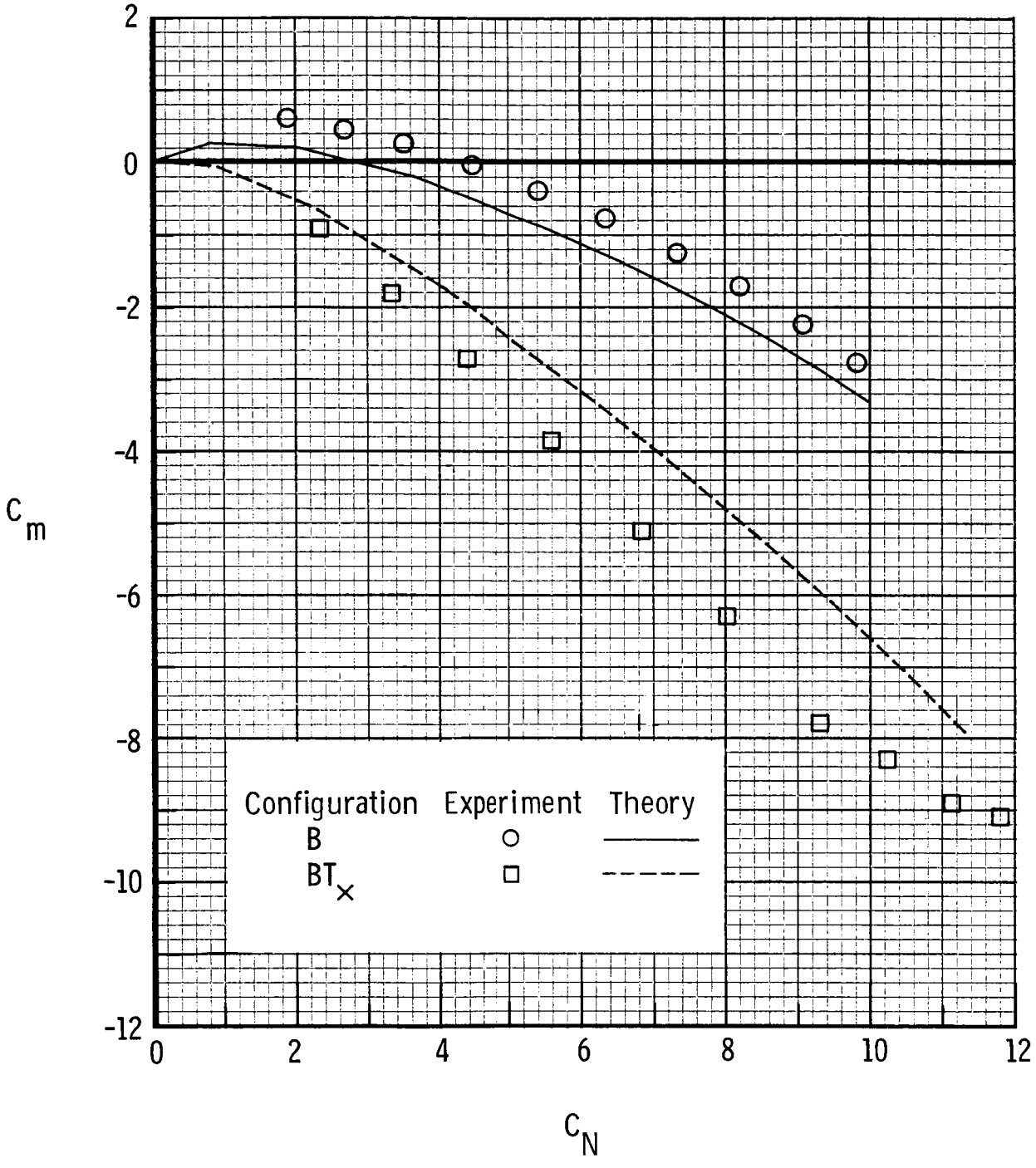

(b) "×" fins.

Figure 8. Concluded.

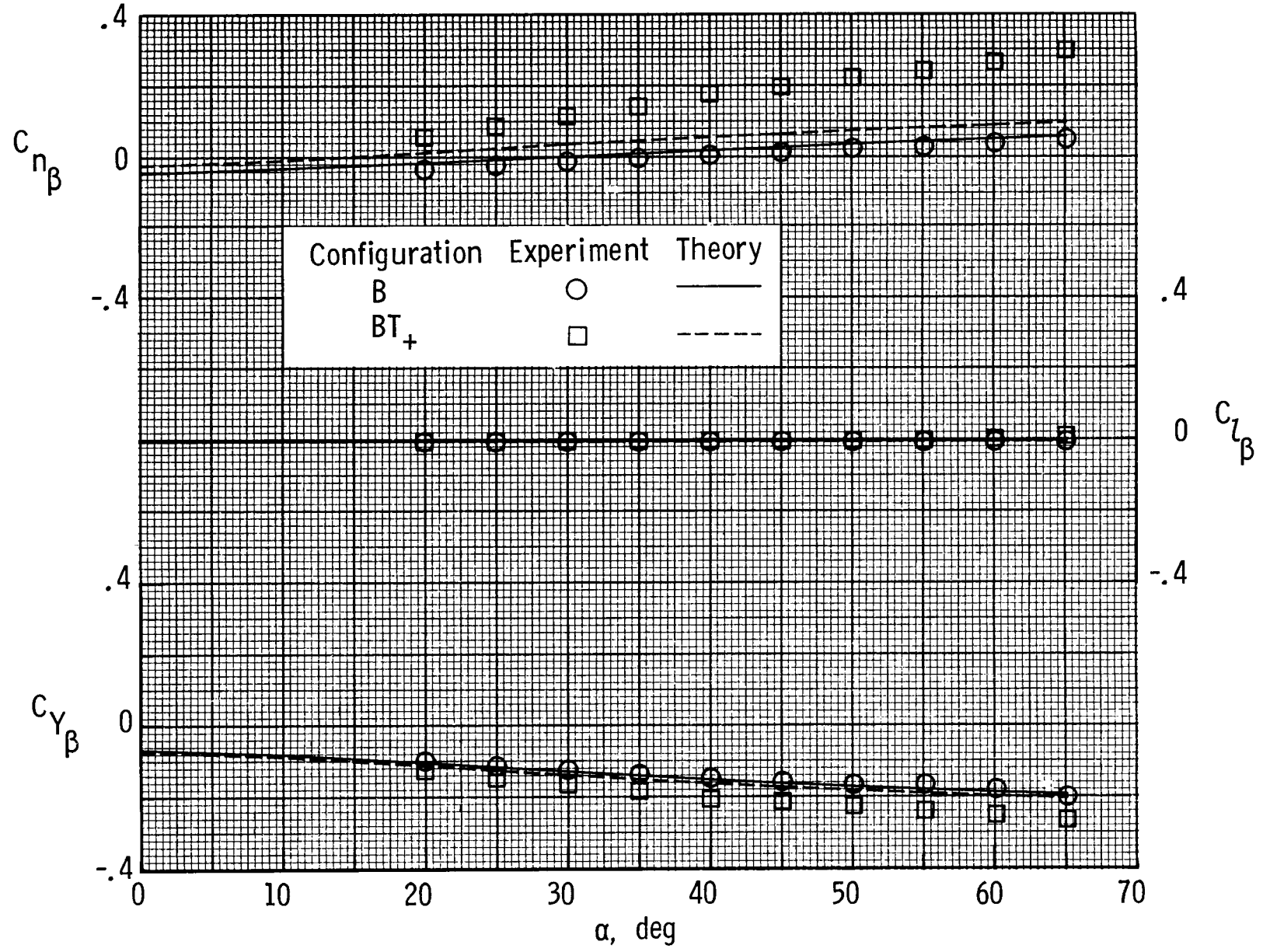

(a) "+" fins.

Figure 9. Effect of component buildup on sideslip derivatives for $\delta_p = 0°$.

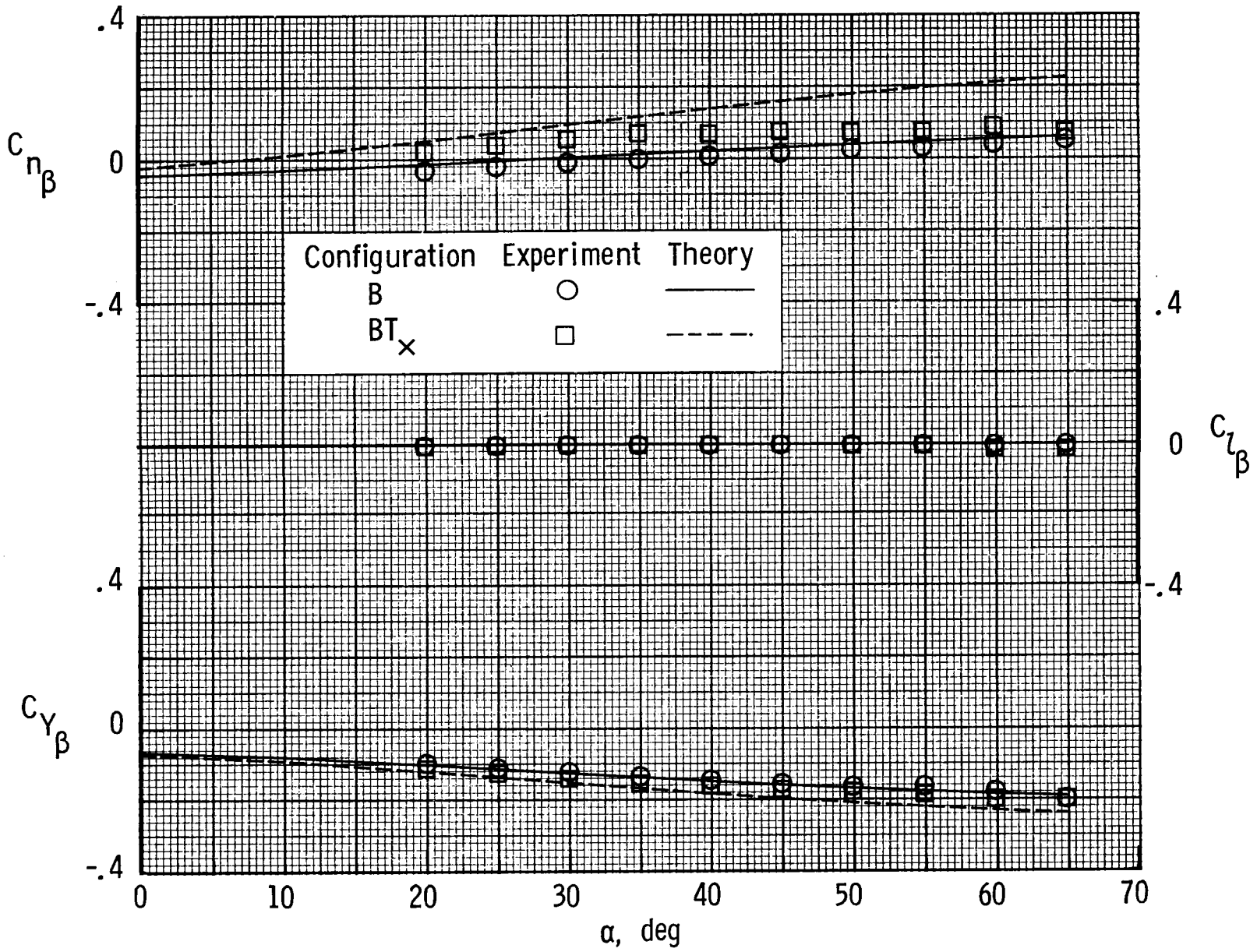

(b) "×" fins.

Figure 9. Concluded.

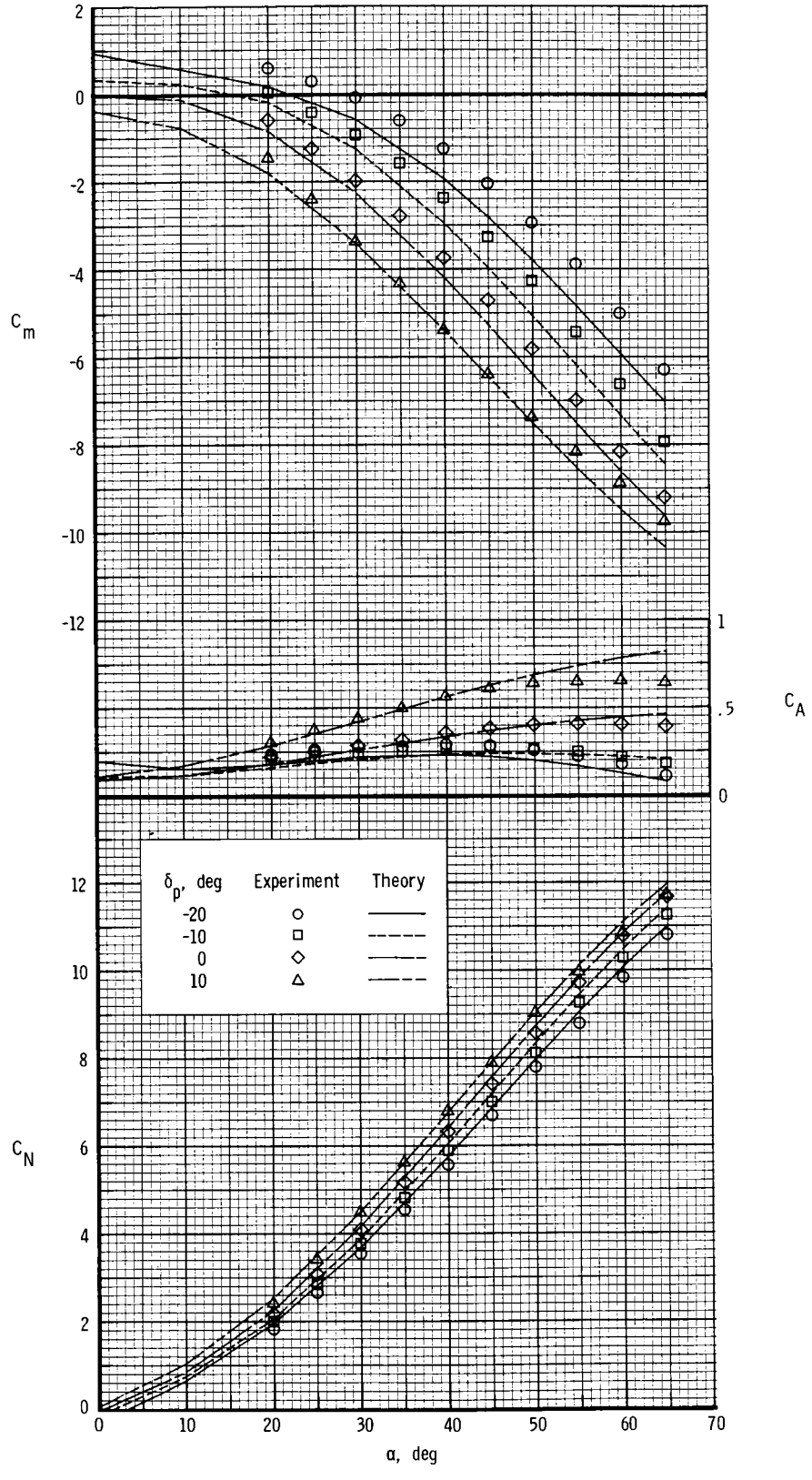

(a) "+" fins.

Figure 10. Effect of pitch-control deflection on longitudinal aerodynamic characteristics.

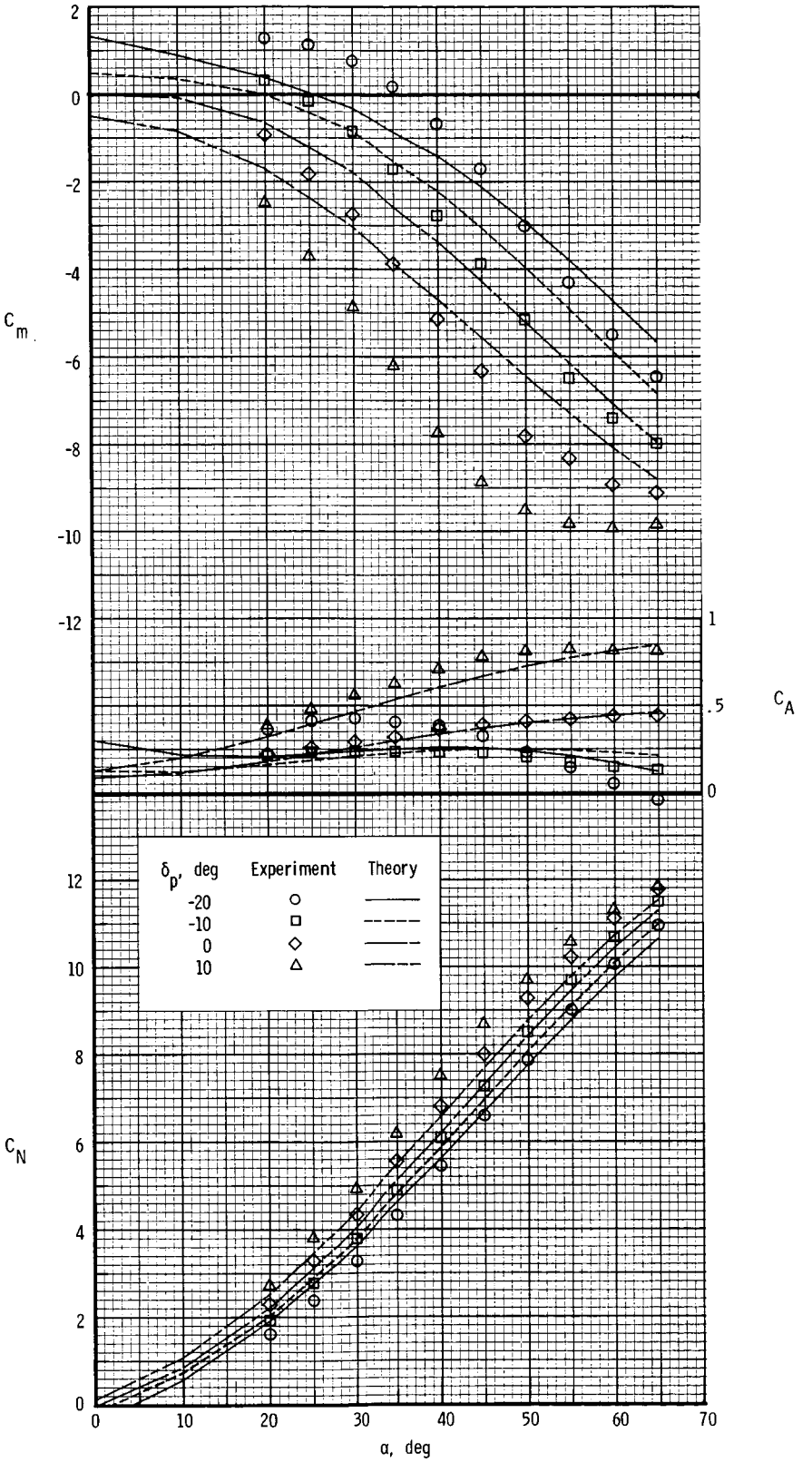

(b) "×" fins.

Figure 10. Concluded.

(a) $\delta_p = 10°$.

Figure 11. Schlieren photographs for "×" fins ($\beta = -3°$).

(b) $\delta_p = -20°$.

Figure 11. Concluded.

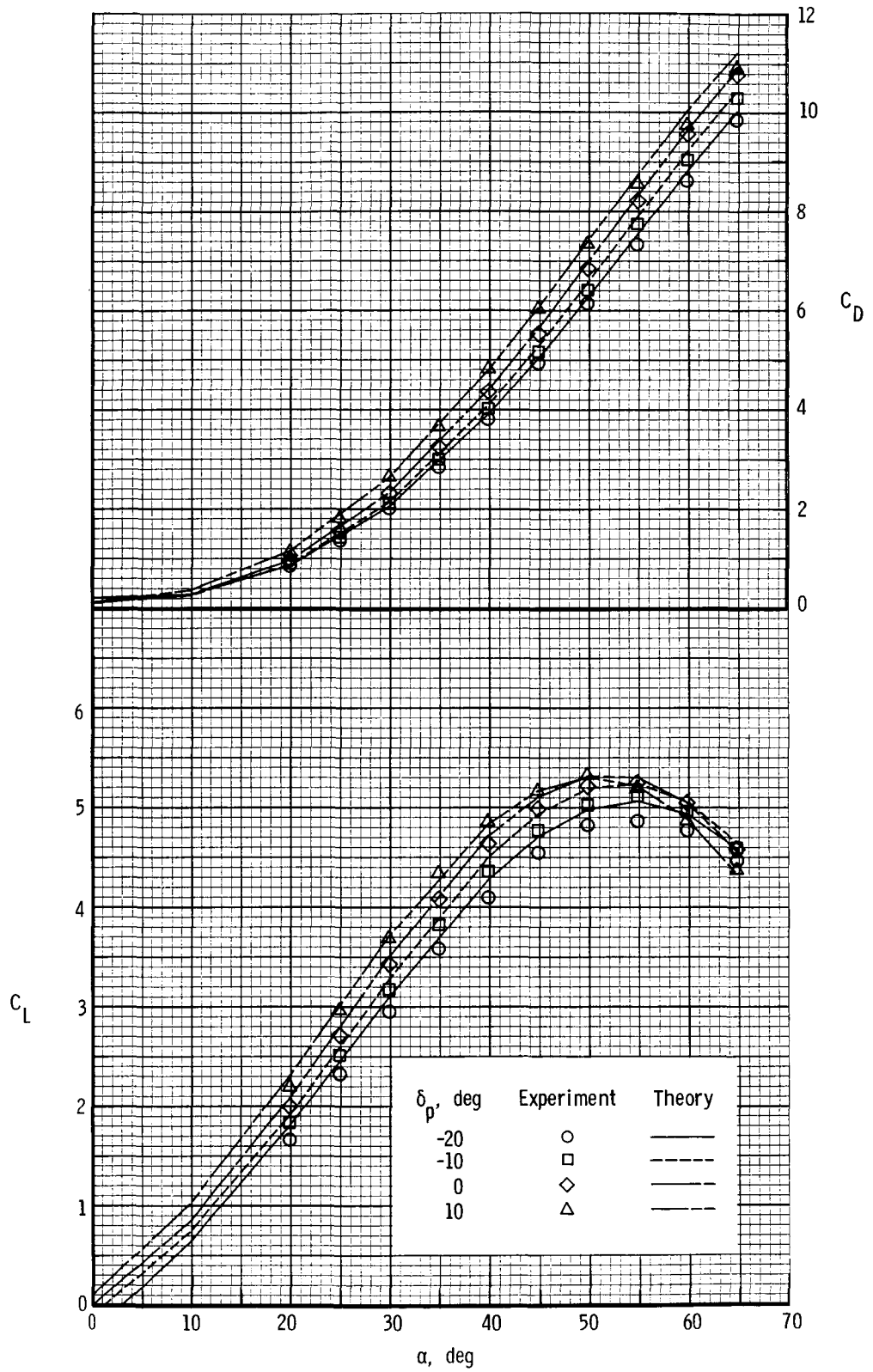

(a) "+" fins.

Figure 12. Effect of pitch-control deflection on performance characteristics.

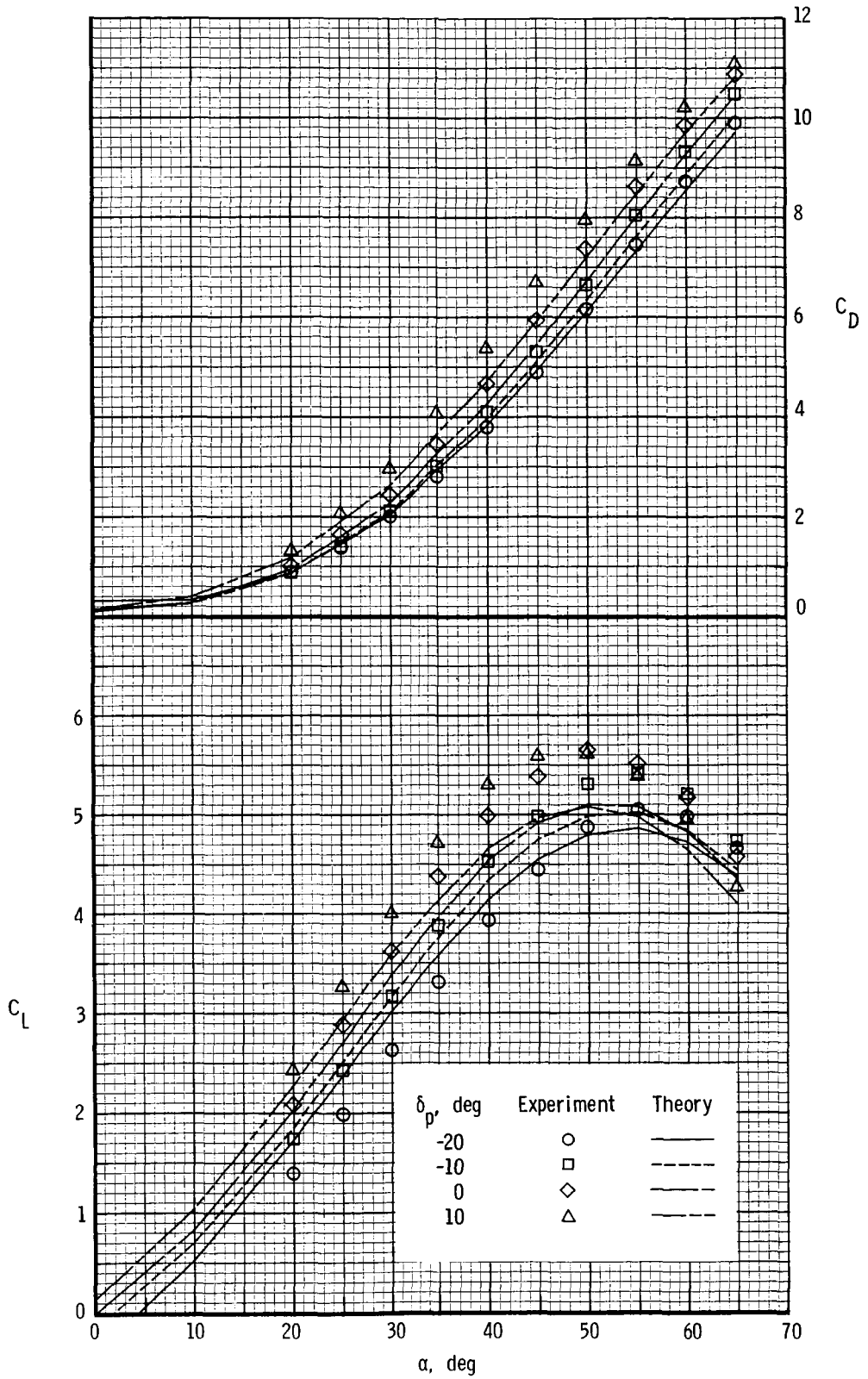

(b) "×" fins.

Figure 12. Concluded.

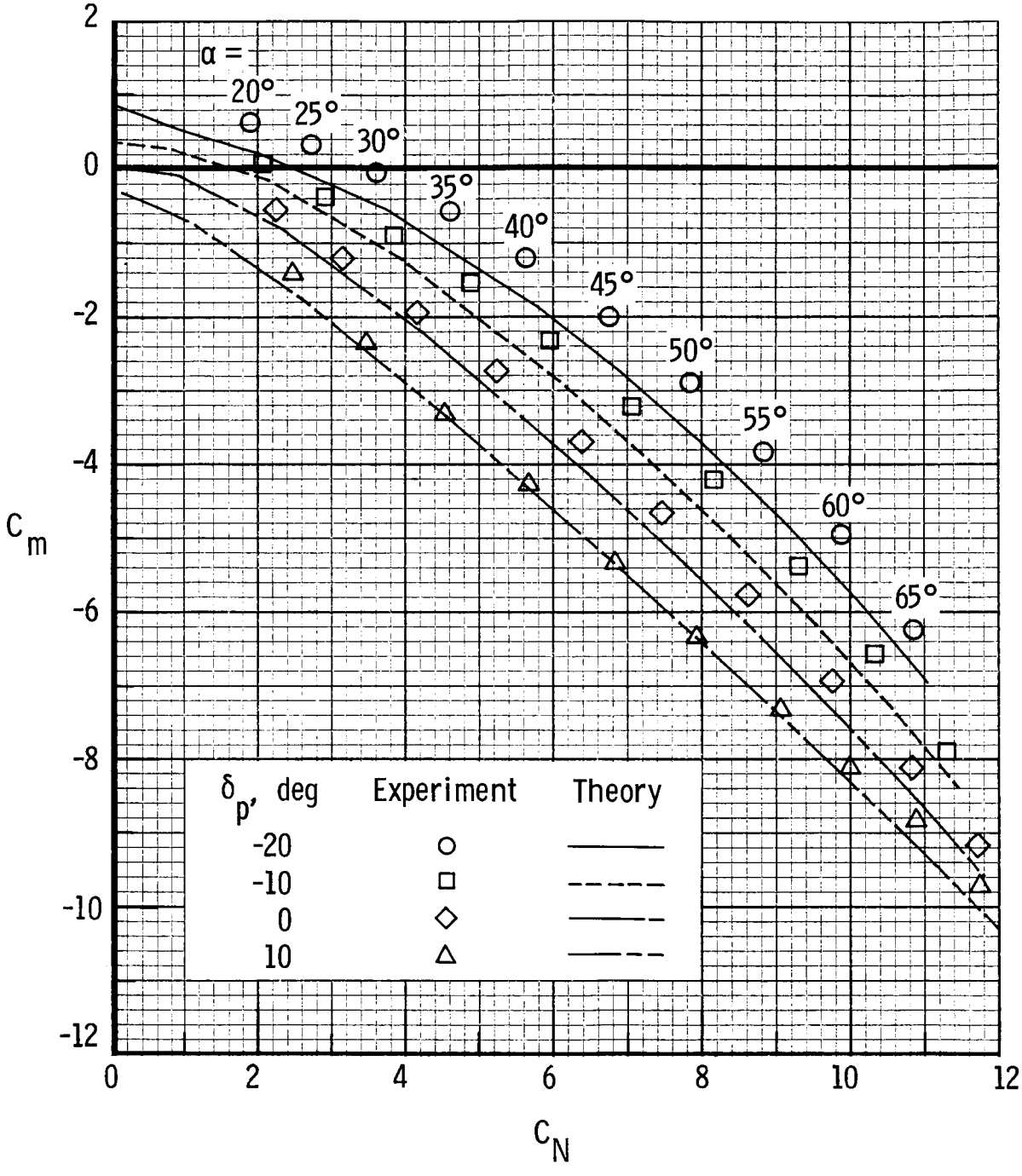

(a) "+" fins.

Figure 13. Effect of pitch-control deflection on longitudinal stability.

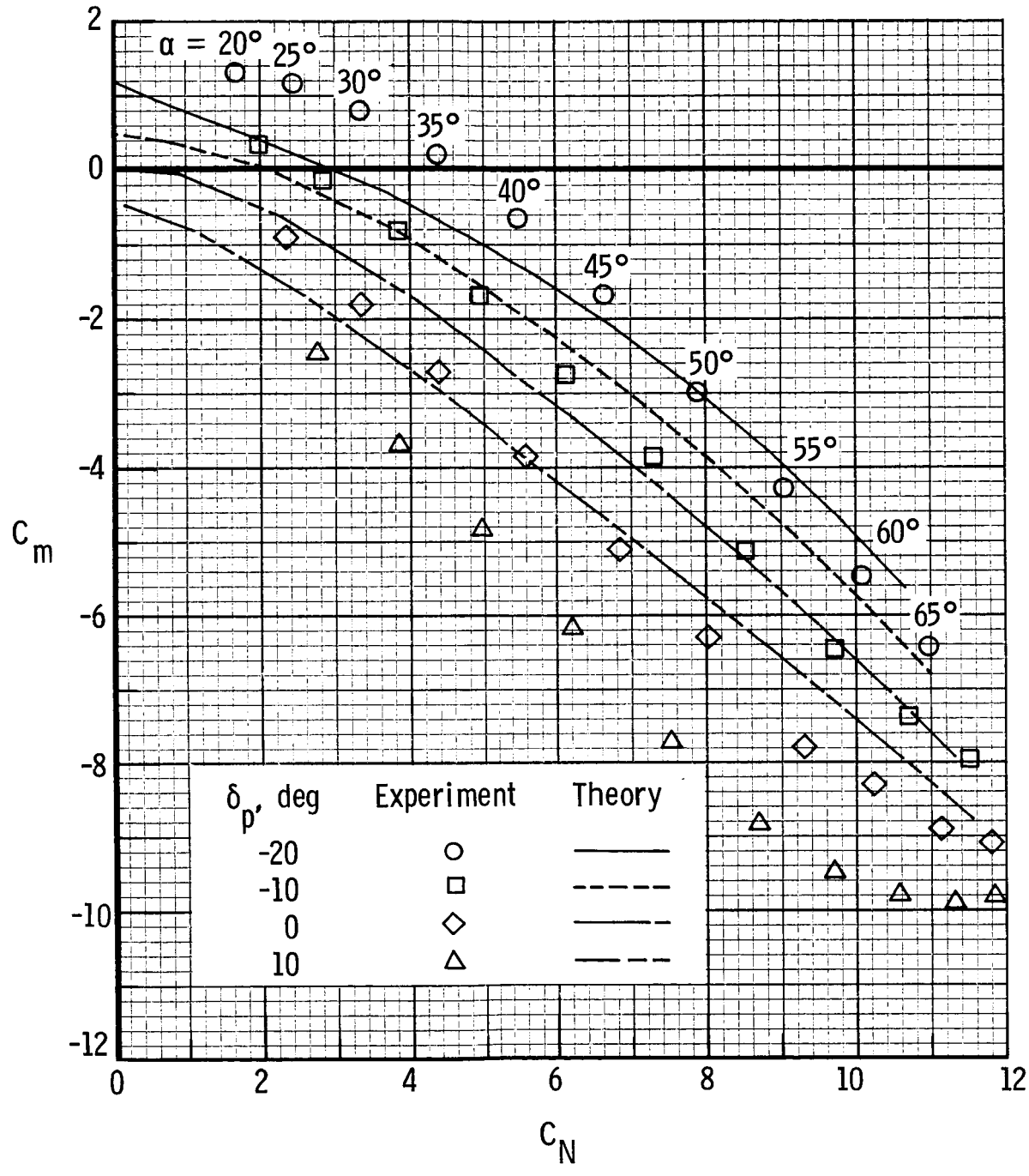

(b) "×" fins.

Figure 13. Concluded.

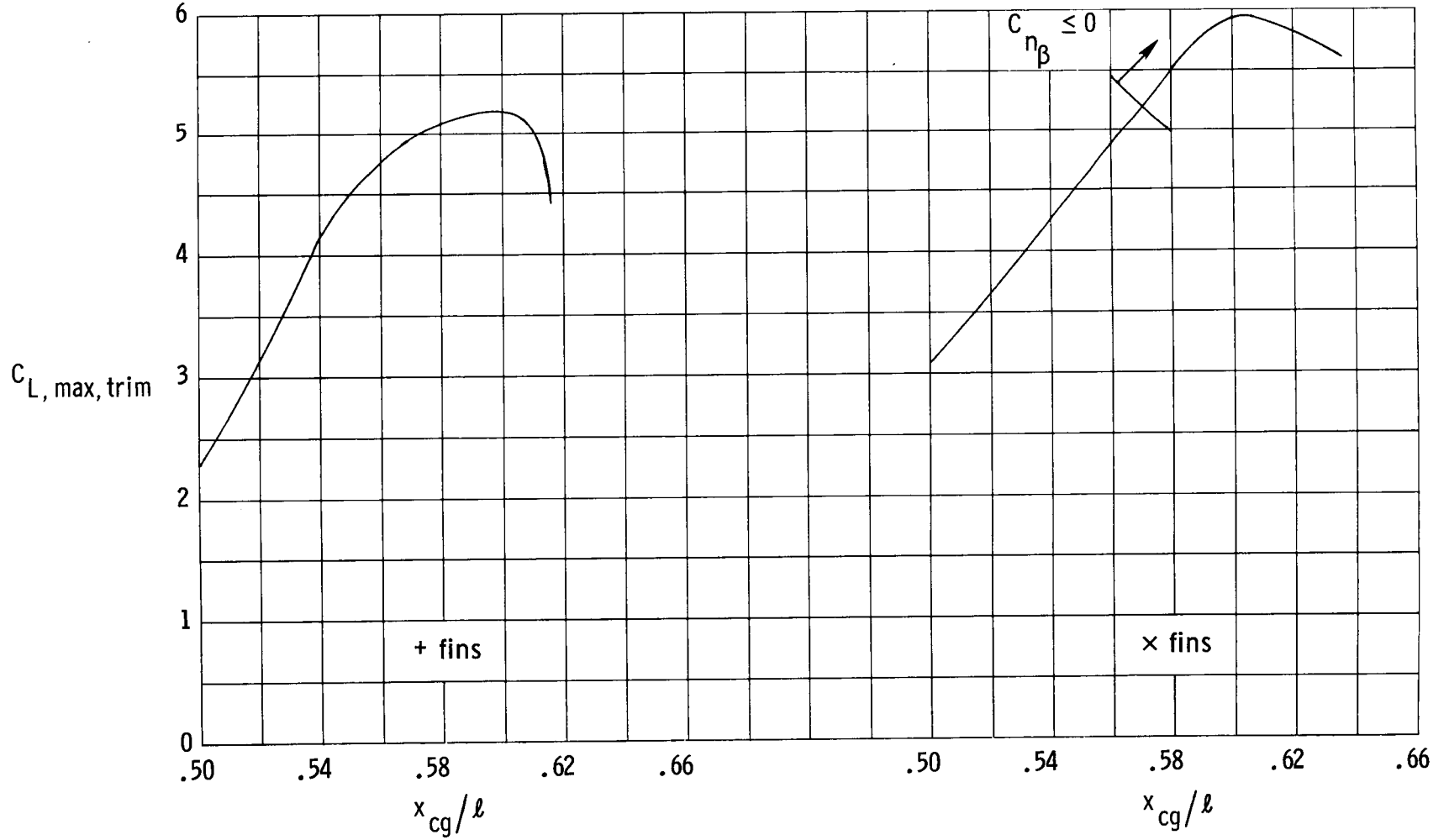

Figure 14. Effect of center-of-gravity location on maximum trimmed lift coefficient.

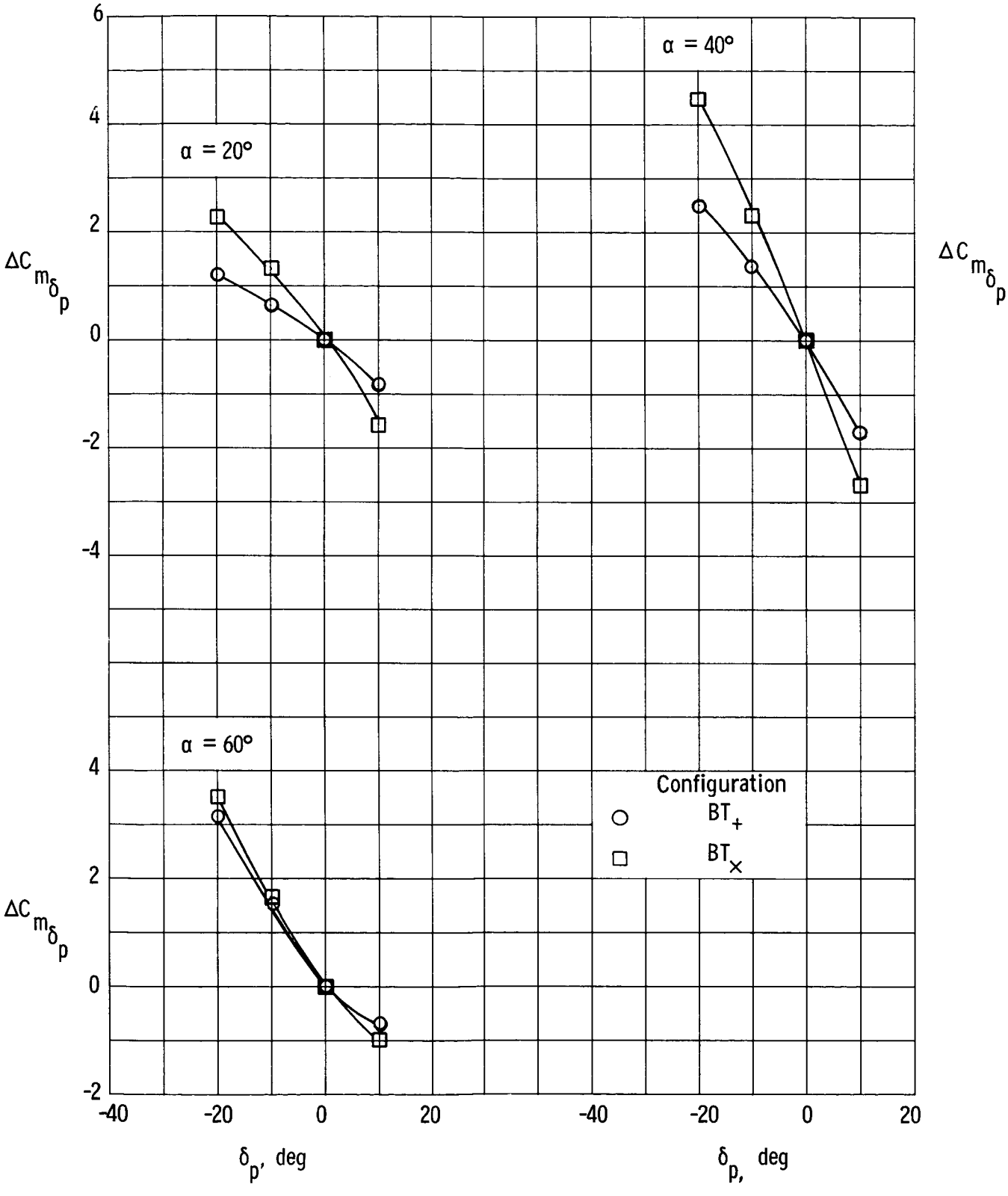

Figure 15. Control power of fins for various angles of attack.

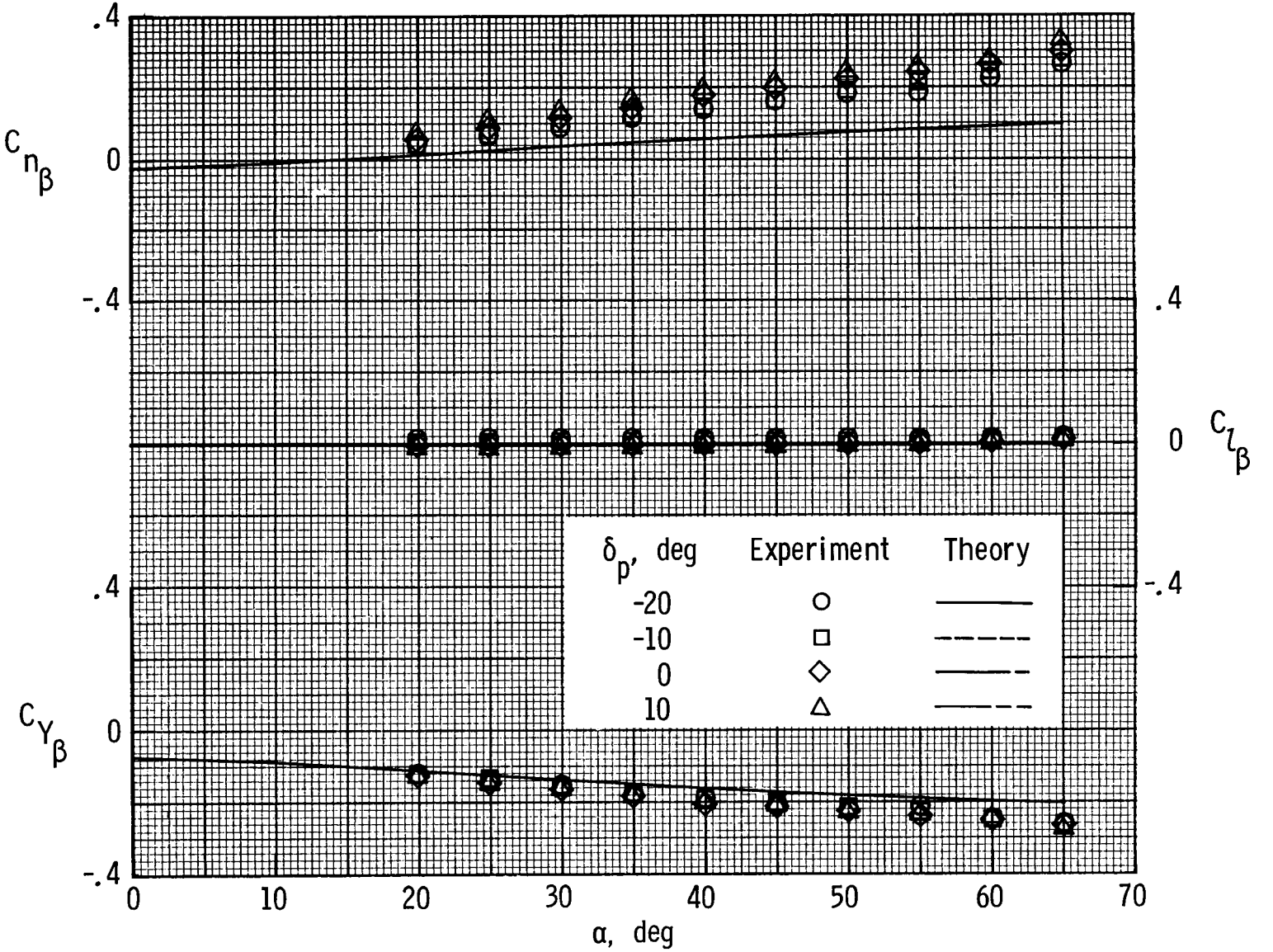

(a) "+" fins.

Figure 16. Effect of pitch-control deflection on sideslip derivatives.

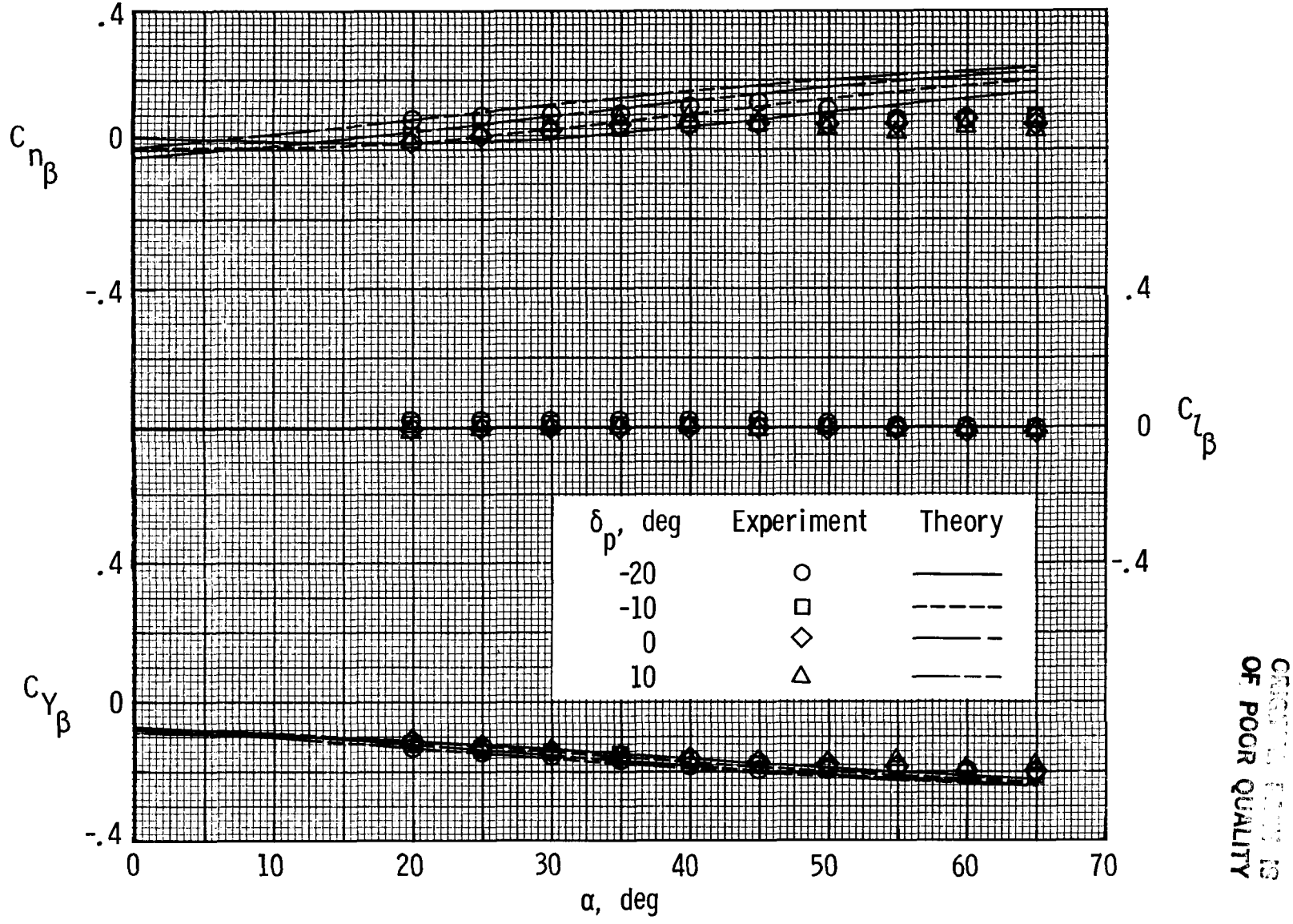

(b) "×" fins.

Figure 16. Concluded.

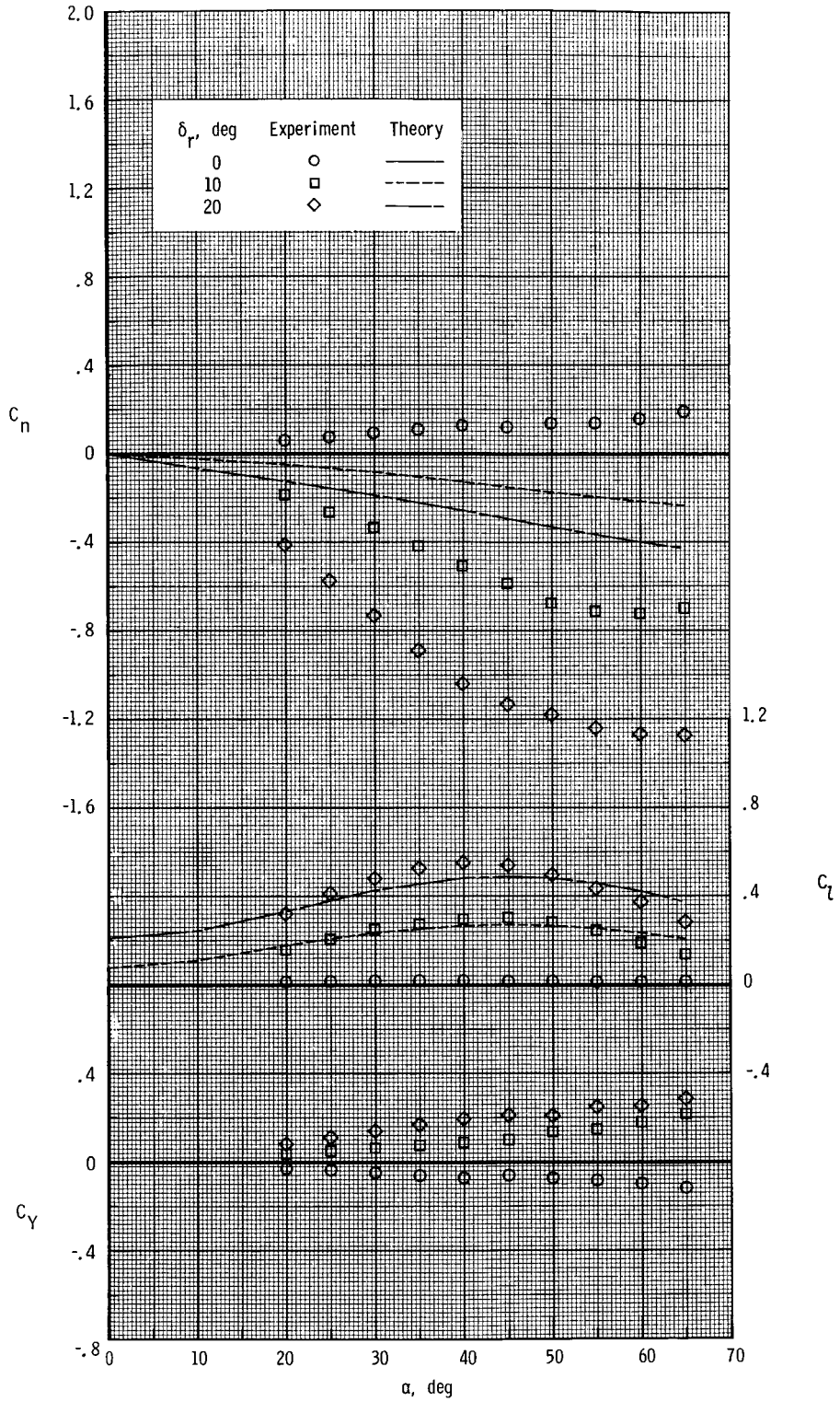

(a) "+" fins.

Figure 17. Roll-control characteristics.

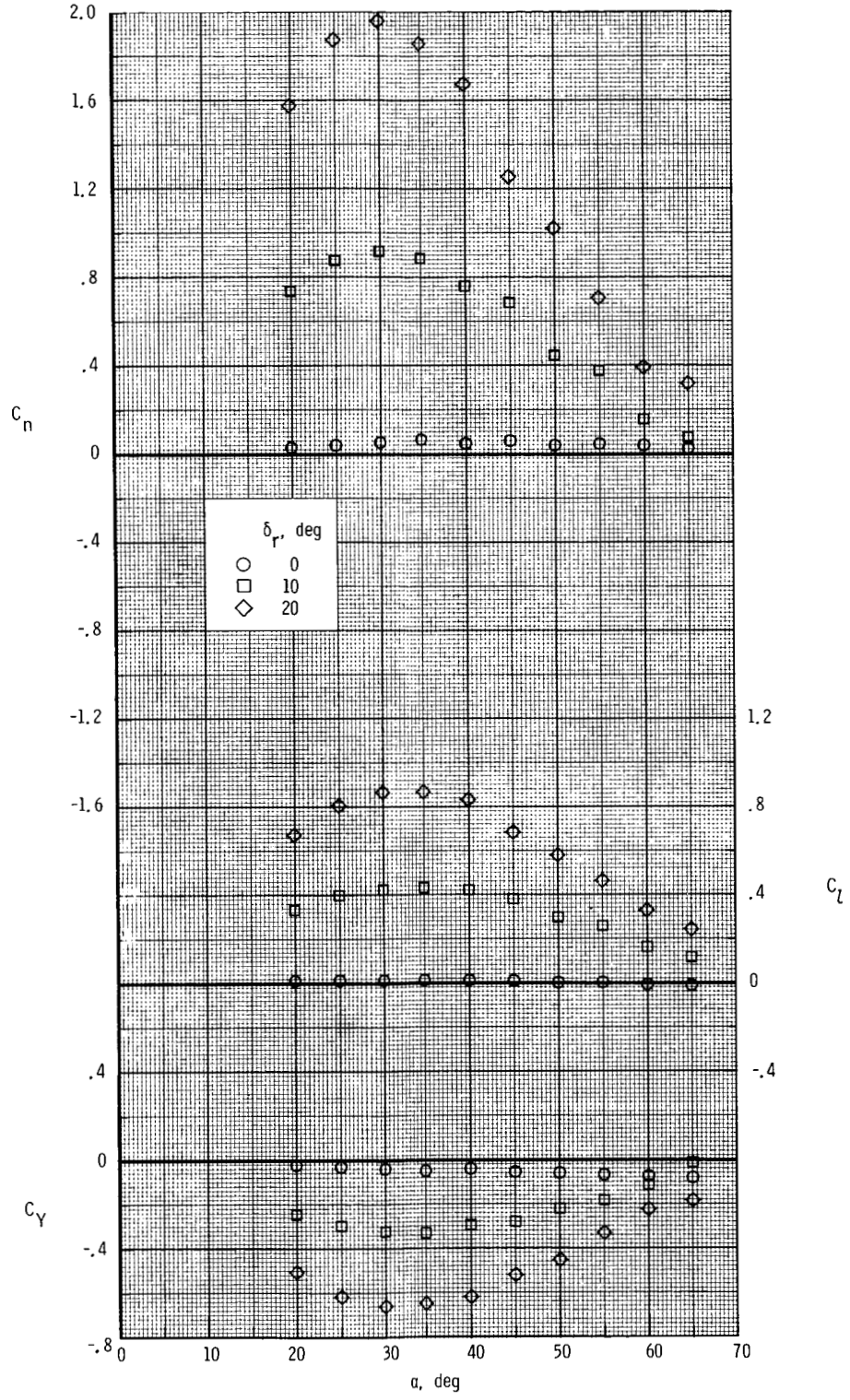

(b) "×" fins.

Figure 17. Concluded.

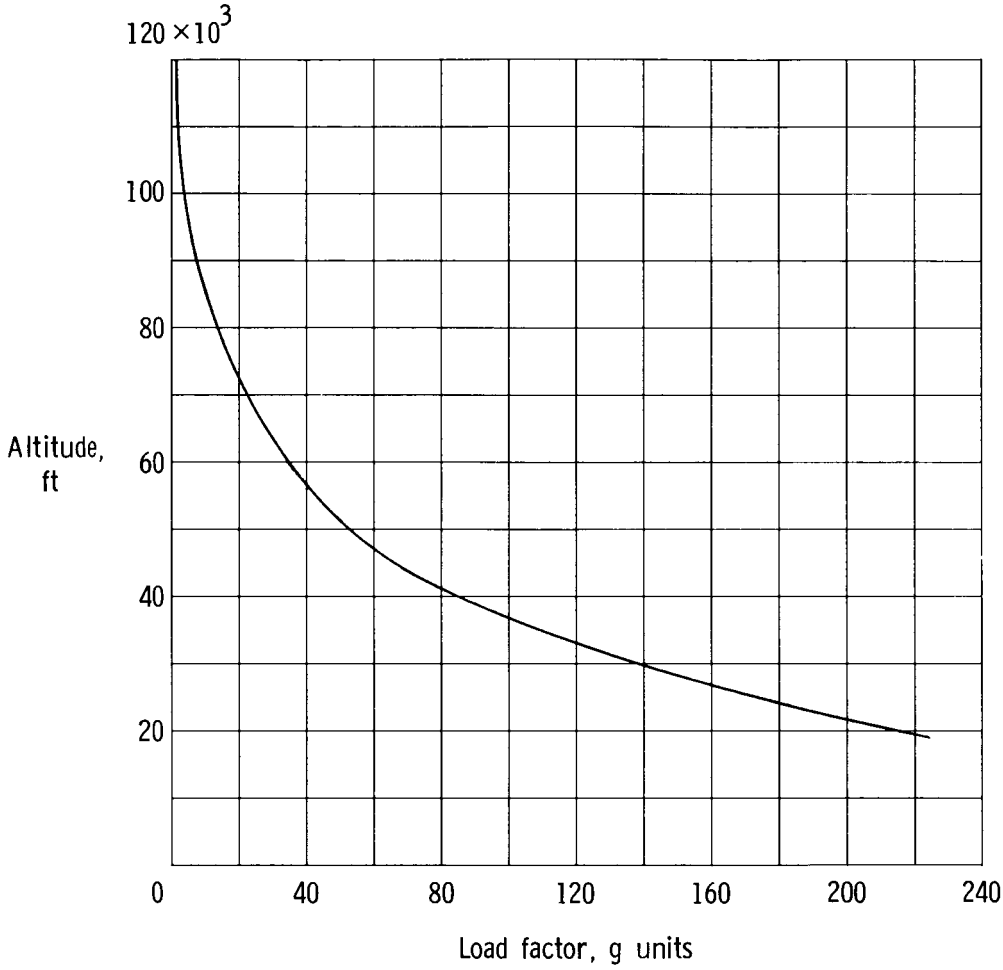

Figure 18. Missile maneuver potential at various altitudes.

NASA
National Aeronautics and Space Administration

Report Documentation Page

1. Report No.	2. Government Accession No.	3. Recipient's Catalog No.
NASA TP-2733		

4. Title and Subtitle	5. Report Date
Mach 6 Experimental and Theoretical Stability and Performance of a Cruciform Missile at Angles of Attack Up to 65°	July 1987
	6. Performing Organization Code
7. Author(s)	8. Performing Organization Report No.
Edward R. Hartman and Patrick J. Johnston	L-16287
9. Performing Organization Name and Address	10. Work Unit No.
NASA Langley Research Center Hampton, VA 23665-5225	505-62-81-07
	11. Contract or Grant No.
12. Sponsoring Agency Name and Address	13. Type of Report and Period Covered
National Aeronautics and Space Administration Washington, DC 20546-0001	Technical Paper
	14. Sponsoring Agency Code

15. Supplementary Notes

Edward R. Hartman: Detailed to NASA from Arnold Engineering Development Center, Arnold Air Force Station, Tennessee.
Patrick J. Johnston: Langley Research Center, Hampton, Virginia.

16. Abstract

An experimental and theoretical investigation of the longitudinal and lateral-directional stability and control of an axisymmetric cruciform-finned missile has been conducted at Mach 6. The angle-of-attack range extended from 20° to 65° to encompass maximum lift. Longitudinal stability, performance, and trim could be accurately predicted with the fins at a fin roll angle of 0° but not when the fins were at a fin roll angle of 45°. At this roll angle, windward fin choking occurred at angles of attack above 50° and reduced the effectiveness of the fins and caused pitch-up.

17. Key Words (Suggested by Authors(s))	18. Distribution Statement
Hypersonic Cruciform missiles Stability and performance High angles of attack Theoretical predictions Fin choking Control authority	Unclassified—Unlimited Subject Category 02

19. Security Classif.(of this report)	20. Security Classif.(of this page)	21. No. of Pages	22. Price
Unclassified	Unclassified	39	A03

For sale by the National Technical Information Service, Springfield, Virginia 22161-2171